Marine Chemistry 201 (2018) 242–255

Contents lists available at ScienceDirect

Marine Chemistry

journal homepage: www.elsevier.com/locate/marchem

The distribution of dissolved and particulate Mo and V along the U.S. GEOTRACES East Pacific Zonal Transect (GP16): The roles of oxides and biogenic particles in their distributions in the oxygen deficient zone and the hydrothermal plume

Peng Ho[a,*], Jong-Mi Lee[b], Maija I. Heller[b,1], Phoebe J. Lam[b], Alan M. Shiller[a]

[a] Division of Marine Science, University of Southern Mississippi, Stennis Space Center, MS 39529, USA
[b] Department of Ocean Sciences, University of California, Santa Cruz, CA 95064, USA

ARTICLE INFO

Keywords:
Molybdenum
Vanadium
Eastern Tropical Pacific
GEOTRACES

ABSTRACT

Molybdenum (Mo) and (V) vanadium are under-studied elements in the ocean due to their largely conservative natures. Thus, no detailed ocean sections of these elements exist although previous reports do suggest possible anomalies in their distributions due to biological, redox, or sorptive processes. Here we present the first detailed ocean sections of dissolved and particulate Mo and V, obtained as part of the 2013 U.S. GP16 GEOTRACES East Pacific Zonal Transect (EPZT) from Peru to Tahiti. Similar to previous work, the distribution of dissolved Mo was largely conservative, while dissolved V showed a ~5% depletion in the upper waters. For dissolved Mo, a small number of samples showed significantly depleted concentrations which, in most cases, gradually increased with time after samples were acidified. This implies the original sample had experienced a partial change in speciation of dissolved Mo from the predominant molybdate to another, as yet, unknown form. In the oxygen deficient zone (ODZ) off the Peru margin, depleted dissolved Mo and V in a few samples corresponded with the nitrite maximum, suggesting the possible involvement of both elements in the nitrogen cycle. Particulate Mo and V enrichments in the ODZ are likely indicative of scavenging by Fe oxyhydroxides and/or biogenic particles. In near surface waters close to the Peru margin, dissolved Mo and V concentrations slightly decreased with increasing total chlorophyll *a*, suggesting the removal of both elements by biological uptake and/or adsorption onto biogenic particles. In contrast to previous reports that removal to reducing coastal/estuarine sediments resulted in surface water depletion of dissolved V, there is no evidence from the EPZT section that this process plays a strong role in the development of the ~5% dissolved V depletion in the surface ocean. Additionally, dissolved V and Mo depletions were seen in some hydrothermal plume waters above the ridge crest, likely due to adsorption onto Fe/Mn oxides and suggesting that these plume waters are a net sink for these two elements. Associations of ridge crest particulate Mo and V with the particulate Mn and Fe carrier phases suggests V was largely scavenged by Fe oxyhydroxides while Mo was likely scavenged by both Fe oxyhydroxides and Mn oxides. Away from the ridge crest, depletions of dissolved V and Mo are seen along the boundaries of the far field hydrothermal plume, though the reasons for this remain obscure. Future studies of these elements could benefit from determination of speciation as well as increased focus on margin areas.

1. Introduction

Molybdenum and vanadium both occur as oxyanions in oxic waters and have somewhat similar geochemical behaviors in the ocean. For instance, both elements are redox-sensitive, with decreased solubility in oxygen-depleted water. Also, Mo and V are micro-nutrients, although their biochemical functions and uptake differ. Conventionally, Mo is thought to be conservative in seawater (Bruland, 1983; Collier, 1985) and V nearly so, with only a ~10% depletion in the shallow ocean relative to deep waters (Collier, 1984; Middelburg et al., 1988; Sherrell and Boyle, 1988). Thus, the distributions of these elements have tended not to be studied in detail in the open ocean and the possibility remains that interesting aspects of their oceanic geochemistries have been overlooked.

The distribution of dissolved Mo is generally thought to be

* Corresponding author.
E-mail address: peng.ho@usm.edu (P. Ho).
[1] Present address: Ifremer, Laboratoire des Cycles Géochimiques, CS 10070, F-29280, Plouzané, France.

https://doi.org/10.1016/j.marchem.2017.12.003
Received 13 October 2017; Received in revised form 4 December 2017; Accepted 15 December 2017
Available online 16 December 2017

essentially conservative in the open ocean (Morris, 1975; Bruland, 1983; Collier, 1985). Likewise, the uniform distribution of Mo stable isotope ratios in the ocean (Nakagawa et al., 2012) also suggests the relative unreactivity of oceanic Mo. However, a number of studies have reported non-conservative behavior of dissolved Mo in coastal and estuarine waters (e.g., Dalai et al., 2005; Dellwig et al., 2007; Joung and Shiller, 2016; Wang et al., 2016). The reasons for this non-conservative behavior are varied and likely relate to biological processes, organic complexation, redox processes, scavenging, and sedimentary interactions. For example, scavenging of Mo by ferromanganese oxides appears to be a mechanism of importance for removal of Mo from the water column (Goldberg et al., 2009; Kashiwabara et al., 2011) and the diagenesis of these oxides plays a role in the enrichment of Mo in reducing sediments (Scholz et al., 2011). Also, the formation of Mo-enriched organic aggregates has been observed to deplete coastal water dissolved Mo (e.g., Dellwig et al., 2007; Kowalski et al., 2013). Mo plays an important biological role in the nitrogen cycle as a co-factor in nitrogenase, nitrate reductase, and nitrite oxidoreductase (Stiefel, 1996; Moreno-Vivián et al., 1999; Maia et al., 2017) as well as in DMSO reductase (Schindelin et al., 1996). Based on thermodynamics, Mo is present in the + VI oxidation state in seawater, predominantly as the highly soluble MoO_4^{2-} species (Baes and Mesmer, 1976; Manheim, 1978). However, small amounts of the more particle-reactive Mo(V), which should be thermodynamically stable in reducing waters (Bertine, 1972; Brookins, 1988), have been reported in low-oxygen estuarine waters (Wang et al., 2009). Furthermore, when there is sufficient sulfide present (~ 11 μM $H_2S_{(aq)}$), molybdate can be sulfidized to more readily scavenged thiomolybdates without reduction of the Mo (Erickson and Helz, 2000; Dahl et al., 2010; Vorlicek et al., 2015). Helz et al. (2011) proposed that the Mo scavenging in sulfidic water is controlled not only by H_2S concentration but also by pH and the availability of reactive Fe(II). This may account for the high levels of Mo found in sediments and pore waters of anoxic depositional environments (e.g., Emerson and Huested, 1991).

As outlined above, the utilization of Mo as an enzymatic co-factor, the interaction of Mo with organic matter, the change of Mo speciation in redox gradients and association with Fe/Mn cycling along with the diagenesis of Mo in sediments/pore waters supports the prior observations of non-conservative Mo behavior in various marginal environments. In the open ocean, however, the limited observations of the Mo distribution are more equivocal. Both slight depletion and enrichment of Mo concentration were reported in the eastern tropical Pacific Ocean by Tuit (2003). However, no significant depletion of Mo was observed either in the extreme oxygen minimum zone (OMZ) of the Arabian Sea (Goswami et al., 2012) or in the eastern tropical North Pacific OMZ (Nameroff et al., 2002). In oceanic hydrothermal systems, Elderfield and Schultz (1996) suggested there was no direct hydrothermal source/sink of Mo, but that scavenging removal in hydrothermal plumes did remove Mo from seawater, albeit at a rate of only ~1% of the fluvial input. However, Mo depletion was observed in vent fluids from the Southern Juan de Fuca Ridge (Trefry et al., 1994). Thus, hydrothermal effects on the oceanic Mo distribution may be variable.

Dissolved V concentrations are generally found to be ~35 nmol/kg in the deep ocean with a slight reduction in concentration in the upper water column (e.g., Collier, 1984; Middelburg et al., 1988; Sherrell and Boyle, 1988). There is one report suggesting deep Pacific concentrations might be 10–15 nmol/kg higher than this (Jeandel et al., 1987), though their intercalibration effort showed somewhat variable results and Middelburg et al. (1988) showed only a few nmol/kg inter-basin increase. Thermodynamically, the predominant species of V in oxic seawater should be $H_2VO_4^-$ (Baes and Mesmer, 1976; Wang and Sanudo-Wilhelmy, 2008), which has similar chemical characteristics as phosphate. Thus, the slight V depletion in surface waters has been attributed to biological uptake of V(V) (Collier, 1984).

V is used as a nutrient by some species (Taylor and van Staden, 1994) and is found in some enzymes (Antipov et al., 1998; Rehder, 2000; Butler and Carter-Franklin, 2004). More specifically, V is found in V-nitrogenases and V-haloperoxidases (Crans et al., 2004). Observation of V-nitrogenase in the ocean may not be likely, since its expression seems to require Mo-limitation (Rehder, 2000). V-haloperoxidases are commonly found in marine macroalgae (Crans et al., 2004). Additionally, previous studies have hypothesized that the intracellular V enrichment in *Trichodesmium* colonies is related to the V-haloperoxidases (Tovar-Sanchez and Sañudo-Wilhelmy, 2011; Nuester et al., 2012). High concentrations of V(III) are also found in certain tunicates (Michibata et al., 2003). While the effect of these types of biological V uptake may be limited, Klein et al. (2013) has speculated on an unknown mechanism of biological V uptake from surface waters based on correlations between intracellular V, biogenic Si, and total chlorophyll *a* and Osterholz et al. (2014) presented evidence that diatoms are a major factor in oceanic V depletion.

In contrast to the biological uptake hypothesis for surface ocean dissolved V depletion, Shiller and Mao (1999) found no evidence of biological V removal in productive waters of the Louisiana Shelf and suggested that V depletion in those shelf waters resulted from V reduction and removal to the sediments. While the details of this mechanism were not specified, it likely involves adsorption of V onto ferromanganese oxide particles, possibly with water column reduction of V(V) to the more readily scavenged V(IV) (Wehrli and Stumm, 1989), and removal to and incorporation into reducing sediments (e.g., Scholz et al., 2011). Thus, an alternative or additional mechanism for surface ocean V depletion might involve V redox chemistry along the continental margins. Other studies have also found dissolved V is lower in concentration in suboxic/anoxic water columns than in oxic waters (Emerson and Huested, 1991; Shiller and Mao, 1999; Wang and Sanudo-Wilhelmy, 2008). Similarly, it has been shown that V is enriched in the solid phase of anoxic and organic-rich sediments (Lewan and Maynard, 1982; Holland, 1984; Breit and Wanty, 1991). Under extremely reducing conditions, V(IV) could be further reduced to V(III) by humic acid or sulfides, and be present as V_2O_3 or $V(OH)_3$ (Goodman and Cheshire, 1975; Breit and Wanty, 1991).

Jeandel et al. (1987) suggested that hydrothermal processes are a minor factor in the cycling of vanadium. However, V has been characterized as an enriched element in hydrothermal vent fluids relative to seawater (German and Von Damm, 2006). Nonetheless, several studies have demonstrated that V is scavenged from seawater and adsorbed onto iron oxyhydroxides within rising hydrothermal plume waters, which is supported by evidence of particulate V enrichments in hydrothermal particles (Trefry and Metz, 1989; Feely et al., 1994; Edmonds and German, 2004). Thus, Elderfield and Schultz (1996) concluded that there is no significant direct hydrothermal input of V to the ocean and that the scavenging removal flux of V from the hydrothermal plumes is roughly equal to the river input flux of V.

Clearly the past work on Mo and V has demonstrated the basics of their oceanic distributions, but uncertainties remain in some of the details. Understanding these details may aid both in understanding modern ocean processes as well as in the interpretation of paleo-environmental data on the ocean's Mo (e.g., Anbar, 2004; Tribovillard et al., 2006; Scott et al., 2008) and V composition (e.g., Hastings et al., 1996; Tribovillard et al., 2006). In this study, we present the first detailed oceanic sections of dissolved Mo and V, obtained along the U.S. GEOTRACES East Pacific Zonal Transect (EPZT). This transect (Fig. 1a) crossed a variety of contrasting oceanic regimes including an extreme OMZ, hydrothermal plumes, and the pelagic realm, thus providing an opportunity to more thoroughly examine the distributions of these two elements.

2. Methods

2.1. Seawater sampling

The U.S. GEOTRACES EPZT was conducted during 25 October–20 December 2013 aboard R/V Thomas G. Thompson from Manta,

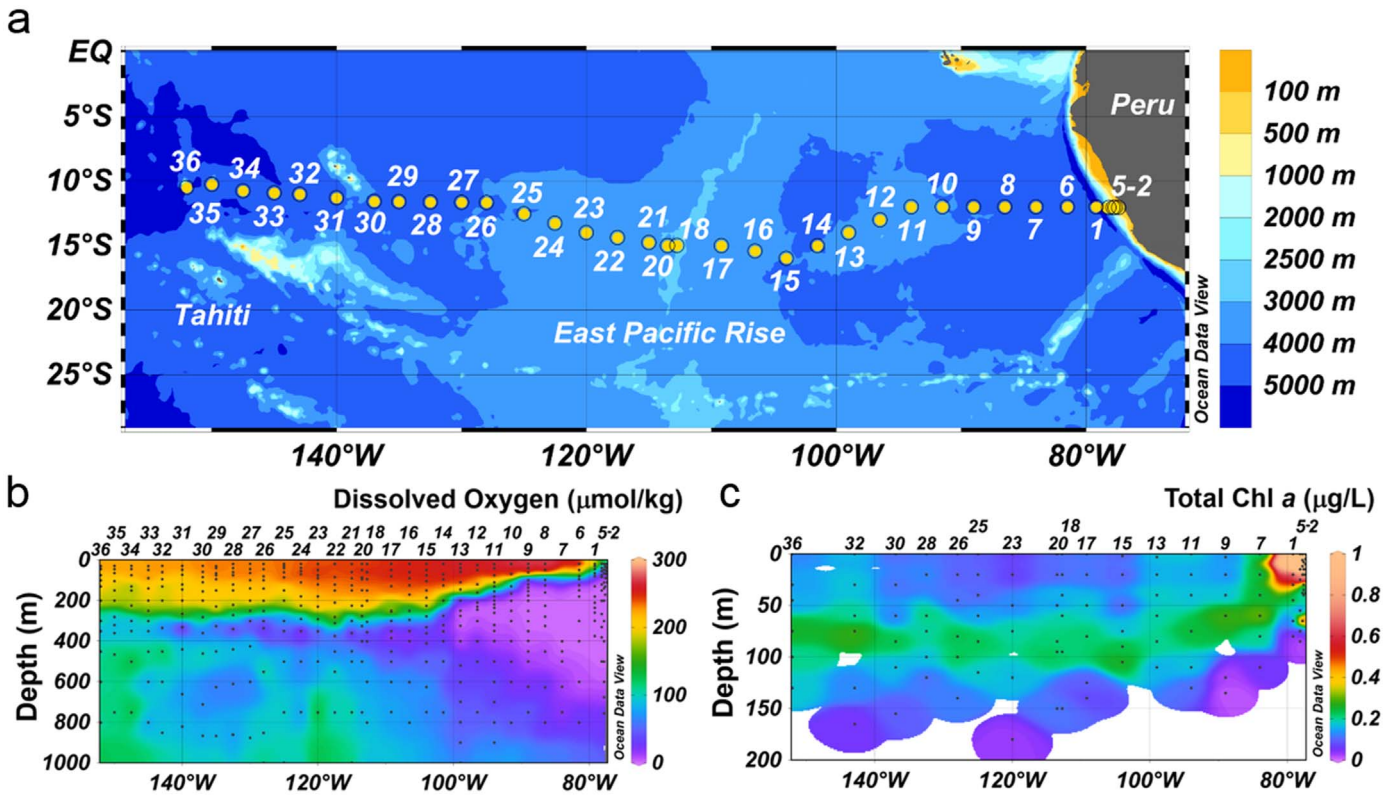

Fig. 1. (a) Cruise track of the US GEOTRACES East Pacific Zonal Section (GP16). Note that station 1 (Peru-Chile Trench) is out of numerical order and is located between stations 5 & 6. (b) The distribution of dissolved oxygen in the upper water column along the EPZT. Purple colour indicates the ODZ. (c) The distribution of total chlorophyll *a* in the upper 200 m of the water column along the EPZT. (For interpretation of the references to colour in this figure legend, the reader is referred to the web version of this article.)

Ecuador to Papeete, French Polynesia (GEOTRACES section GP16; Fig. 1a). Samples were collected at four shelf stations (1–2 casts), 13 full depth stations (3 casts), 13 shallow stations (1 cast, depth ~ 1000 m) and five super-stations (3–4 casts) by use of 12-L Teflon-coated GoFlo bottles deployed on the trace metal clean GEOTRACES carousel (Cutter and Bruland, 2012).

Water samples were filtered through 0.2 µm capsule filters (Pall Acropak Supor capsule) and collected by an ultra-clean sampling technique which was previously deployed during CLIVAR (Measures et al., 2008) and U.S. GEOTRACES intercalibration and North Atlantic cruises (Cutter et al., 2014). In addition, surface water samples (~2 m depth) were taken from an underway towed-fish system (Bruland et al., 2005) and filtered through a 0.45 µm Osmonics and a 0.2 µm polycarbonate cartridge filter.

The filtered samples (~125 mL) collected from the GoFlo bottles were stored in pre-cleaned HDPE bottles and shipped back to the laboratory for acidification and analysis. Ancillary data (e.g., salinity, temperature, nutrients, oxygen) was provided by the cruise management team (http://www.bco-dmo.org/project/499723). After samples were transported to the laboratory, an aliquot of ultrapure 6 N HCl (Seastar Baseline) was added to each sample to reduce the pH to ~1.8 and the samples were then stored at room temperature.

2.2. Particle sampling

Particle samples were collected at four shelf stations, 13 full depth stations and five super-stations. Here, we briefly describe particle sampling protocols. Two particle fractions (small size fraction: 0.8–51 µm; large size fraction: > 51 µm) were collected using McLane WTS-LV in-situ battery powered pumps that were deployed on a metal-free hydrowire (Hytrel-jacketed Vectran). Filters were loaded in two mini-MULVFS filter holders ("QMA' and 'Supor') (Bishop et al., 2012) which were configured with each pump. All filters were acid leached (Cutter et al., 2014) in a HEPA-filtered clean environment prior to use. Each filter holder held a 142 mm-diameter, 51 µm pore-size polyester pre-filter, and either a pair of Whatman QMA quartz fiber filters or a pair of 0.8 µm pore-size Pall Supor™ polyethersulfone filters. In each cast, blank filters (both "QMA" and "Supor") that were not connected to the pumps were deployed together with the pumps, and these dipped blank filters were treated as procedure blanks. After the pumps were recovered, the filter holders were brought into a shipboard HEPA-filtered clean environment for rinsing, subsampling and drying procedures and then stored in particle-free cleanroom polyethylene bags. More detailed particle sampling protocols are described in Heller et al. (2017), Lam et al. (2017), Lee et al. (2017) and in on-line documentation (http://www.bco-dmo.org/project/499723).

2.3. Analytical methods

2.3.1. Dissolved Mo and V

Both dissolved Mo and V were determined using a ThermoFisher Element XR sector field inductively coupled plasma-mass spectrometer (ICP-MS) with a PFA microflow nebulizer (Elemental Scientific, Inc.). Quantification used the isotope dilution method. We obtained enriched ^{95}Mo (96.45%) and ^{50}V (44.30%) from Oak Ridge National Laboratories. In general, we sought to spike the samples with an amount of enriched isotope such that measured isotope ratios in the spiked sample were close to the geometric mean of the natural isotope ratio and the isotope ratio of the enriched spike.

For Mo, ~50 µL of seawater was spiked with ^{95}Mo and diluted 30-fold with ultrapure water prior to ICP-MS analysis using a PFA spray chamber (Shim et al., 2012). The intensities of ^{95}Mo and ^{98}Mo were determined in low resolution on the ICP-MS. We measured Br during analyses to check the interference of $^{79}Br^{16}O^+$ and $^{81}Br^{17}O^+$ on ^{95}Mo and ^{98}Mo, respectively. The correction for BrO^+ was usually < 1% (1.1 nmol/kg) and not > 2.5% (2.7 nmol/kg). The reproducibility of

Table 1
Reproducibility of dissolved Mo and V in GEOTRACES reference waters and detection limits for Mo and V. The recovery of V was calculated by a standard addition method.

	Mo	V
GS (nmol/kg)	115.3 ± 2.2 (N = 17)	34.5 ± 0.5 (N = 16)
GD (nmol/kg)	111.4 ± 2.3 (N = 18)	32.9 ± 0.5 (N = 16)
[a]Avg. replicate deviation (nmol/kg)	2.3	0.7
Recovery (%)		99.5 ± 2.8 (N = 31)

[a] Average absolute deviation in 32 pairs of replicates.

this method was estimated by comparing samples collected at the same depth on different casts at the same station. For 32 pairs of these replicate samples, the average absolute deviation was 2.3 nmol/kg or typically 2.1% (Table 1). Repeated runs of U.S. GEOTRACES intercalibration samples (GS and GD; Table 1) and in-house reference solutions suggest a precision of ± 2.3% (Table 1); the limit of detection for Mo was ~1 nmol/kg. Average Mo of GS and GD in our analyses were comparable to reported Mo values (GS: 116 nmol/kg; GD: 113 nmol/kg) by Goswami et al. (2012).

For V, 14-mL samples were spiked with a ^{50}V–enriched solution and extracted/preconcentrated in 1 mL of eluate (10% HNO_3, Seastar Baseline) by using an Elemental Scientific (ESI) seaFAST system. Multiple elements can be simultaneously extracted using the chelating resin Nobias PA-1 (Sohrin et al., 2008; Biller and Bruland, 2012) which is the extraction material used in the seaFAST system. This system removes the matrix effect caused by seawater major ions while a buffered (NH_4Ac) sample passes through the Nobias PA-1 extracting many trace metals but excluding major seawater ions. The seaFAST also avoids the problem of ICP-MS interface clogging caused by sea salt or $Mg(OH)_2$ precipitates. A similar online seaFAST extraction procedure is described by Hathorne et al. (2012) for rare earth elements. Eluates from the seaFAST system were analyzed in medium resolution on the ICP-MS using an Apex-FAST high efficiency sample introduction system with Spiro desolvator (Elemental Scientific, Inc.) to obtain the intensities of ^{50}V and ^{51}V. Additionally, ^{47}Ti and ^{52}Cr were monitored to correct for any ^{50}Ti or ^{50}Cr isobaric interference on ^{50}V; the correction was generally < 1%. The reproducibility of this method was estimated by comparing samples collected at the same depth on different casts at the same station. For 32 pairs of these replicate samples, the average absolute deviation was 0.7 nmol/kg or typically 2% (Table 1). Repeated runs of U.S. GEOTRACES intercalibration samples (GS and GD; Table 1) and in-house reference solutions suggest a precision of ± 1.5%; the limit of detection for V was ~0.5 nmol/kg. Recovery of the method, as determined by repeated analysis of a spiked and unspiked seawater sample was 99.5 ± 2.8% (Table 1).

Because dissolved Mo and V are conservative or nearly so, much of the variability in the concentrations of these elements is caused by changes in salinity. We thus normalized our concentrations to constant salinity for this presentation by dividing by the in situ salinity and multiplying by 35. To present the spatial distribution of dissolved Mo (dMo) and V (dV), we used the Ocean Data View software package (Schlitzer, 2015).

2.3.2. Particulate Mo and V

Methodological details for particulate trace element analysis are in Lee et al. (2017) and Heller et al., 2017. Briefly, subsamples of small (0.8–51 μm) and large (> 51 μm) size fraction particulate samples collected by in-situ filtration were digested using a two-step digestion method that first fully dissolved the polyethersulfone filter using the strongly oxidizing Piranha reagent (75% H_2SO_4/25% H_2O_2), and then fully dissolved particles in a strong mineral acid mixture of 4 M each of HCl, HNO_3, and HF (Ohnemus et al., 2014). Digest solutions were diluted and analyzed for a suite of elements on an ElementXR sector field ICP-MS in the UCSC Plasma Analytical Facility. To verify the accuracy of analytical procedures, two certified reference materials (CRMs), BCR-414 (freshwater plankton) and PACS-2 (coastal marine sediment), were digested and analyzed using the same procedures as for samples. The average recoveries of BRC-414 for Mo and V were 110 ± 10% and 112 ± 11%, respectively. The average recoveries of PACS-2 for Mo and V were 89 ± 13% and 92 ± 8% respectively.

Table 2
The median and standard deviation of dipped blanks and detection limit for both small and large fractions of particulate Mo and V. There were 46 blank filters for small size fraction and 44 blank filters for large size fraction. The dipped blank values are for the entire area of the filters (active area = 125 cm^2). The detection limit was defined as three times the standard deviation of the dipped blank filters. Dipped blanks and detection limits in pM were derived by assuming seawater volumes filtered through small size filters (470 L) and large size filters (1100 L).

	Small size fraction		Large size fraction	
	Mo	V	Mo	V
Median of dipped blank (pmol)	308	178	130	67
s.d. of dipped blank (pmol)	65	52	95	71
Approx. dipped blank (pM)	0.76	0.44	0.12	0.06
Approx. detection limit (pM)	0.48	0.38	0.26	0.19

Reported particulate Mo and V concentrations in this manuscript were corrected with the median of all dipped blanks, filtered seawater volume and the filter area used in digestion. The median dipped blank values and the detection limits for Mo and V are shown in Table 2. The uncertainty of particulate Mo and V concentrations can be attributed to the dipped blank correction, heterogeneity in particle distribution, and variation in digestion. The uncertainty for most samples was mainly from the blank correction. For the large size particulate Mo (pMo), most samples were below detection and thus only the small size fraction pMo is discussed here, with the exception of ridge crest hydrothermal samples where the large fraction pMo was significant. In contrast, for particulate V (pV) the large size fraction accounted for a wide range of the total particulate V (0.7–82%) but was typically only 16% (median) of the total across the section (Lee et al., 2017). Thus, in general, particulate V in our discussion refers to the small particulate fraction; where necessary, we do distinguish the behavior of large particulate V when its contribution becomes significant.

In order to help identify the composition/origin of particulate trace elements, we calculated their non-lithogenic fractions. This was done by assuming that all particulate Al was lithogenic in origin. We then used element/Al ratios for upper continental crust (Rudnick and Gao, 2014) to estimate the amount of a particulate element likely to be of lithogenic origin. Non-lithogenic fractions were then estimated by subtracting the lithogenic estimate from the total particulate elemental concentration.

All original data, ancillary data (salinity, nitrite, density, total chlorophyll *a* and dissolved oxygen) and total particulate elements data are available online at BCO-DMO (http://www.bco-dmo.org/project/499723).

2.4. Reanalysis of depleted dissolved Mo and V samples

Lower than expected dMo and dV concentrations were measured in a few samples. Because of the large number of samples in the EPZT section, we only re-analyzed dMo when the initial sample analysis was more than two standard deviations (5 nmol/kg) from the section salinity-normalized mean. For dV, we chose samples with dV < 30 nmol/kg for re-analysis. Low dV in these samples was reproducible in the re-analysis. In order to verify that the dMo depletions were real, the Mo-depleted samples were re-analyzed a number of times (2–5 times) over 19 months. An additional reanalysis was performed if the first two results disagreed by more than two standard deviations. In general, we averaged all results except when one of the three analyses was more than three standard deviations away from the other two. An interesting

phenomenon was found in many of these Mo-depleted samples. We observed that dMo in most of the Mo-depleted samples increased with sample storage time (~19 months). This observation is discussed in more detail below in Section 3.2. For the samples with slowly changing concentrations, the values reported here are averages of all replicate analyses of that sample since we do not know what the initial depleted value was. In other words, our presentation of those depleted concentrations is necessarily semi-quantitative. Acknowledging the imprecision of our terminology, we will refer to these samples as "Mo-depleted." When the salinity-normalized Mo was > 3 standard deviations from the section mean dMo (i.e., < 101.1 nmol/kg), the depletion was viewed as significant.

3. Results and discussion

3.1. Oceanographic setting and ancillary data

Peters et al. (2017) reported nutrients, hydrographic data, and the distribution of water masses in the EPZT. We review here a few of their most pertinent conclusions relating to hydrographic and nutrient features. The lowest surface water temperature (~15 °C) was found near the Peruvian coast, indicating upwelling of offshore cooler waters. A pool of high salinity water at ~100 m depth in the mid-section originated from subtropical gyre water. A salinity minimum in the mid-water column (600–800 m) reveals the influence of Antarctic Intermediate Water in this region. Warmer and slightly fresher deep waters (> 3000 m) east of the East Pacific Rise (EPR) reflect the signature of Pacific Deep Water (PDW). West of the EPR, slightly cooler and saltier deep water was influenced by Antarctic Bottom Water. More detailed hydrographic data are presented in the Water Mass Analysis manuscript in this issue (Peters et al., 2017).

Typical nutrient profiles were observed in the EPZT (Peters et al., 2017). Nitrate and phosphate were low in the upper water column and reached maximum concentrations at ~800 m, then, slowly decreased with depth. Silicic acid increased with depth, except for a slight decrease in bottom waters in the western part (Stns. 32–36) and eastern part (Stns. 1–9) of the transect. An extreme OMZ (dissolved oxygen < 2 μmol/kg) was observed from the Peruvian coast to at least 100°W (Stns. 1–13) (Fig. 1b), which can be attributed to weak ventilation and consumption by intense biological activity (Karstensen et al., 2008; Peters et al., 2017). For clarity and to distinguish the normal oceanic oxygen minimum zone from this extreme zone, we use the term oxygen deficient zone (ODZ) to refer to the region of the water column with essentially anoxic conditions. In the case of the EPZT, the ODZ was found from Stn. 13 east to the Peru margin. Nitrite enrichments in the ODZ have previously been mainly attributed to nitrate reduction and ammonia oxidation (Lam et al., 2009). In deep water (> 3000 m), lower oxygen and higher silicic acid east of the EPR than to the west suggests the influence of PDW on the tropical eastern Pacific deep basin. More detailed nutrient results were discussed in the water mass analysis manuscript (Peters et al., 2017).

High total chlorophyll *a* (Chl *a*) concentration was seen in surface waters (0–25 m) near the Peruvian coast (Stns. 1–5) (Fig. 1c), implying high primary productivity in that region. Pigment composition showed macroplankton dominance at coastal stations (Stns. 1–5) which shifted to picoplankton dominance in the open ocean (Ohnemus et al., 2017). Heading to the open ocean (west of 100°W), the total Chl *a* maximum occurred at depths of 75–100 m (Fig. 1c; Ohnemus et al., 2017). The depth of the total Chl *a* maximum was tilted slightly upward toward the coast (east of 100°W) where the region was more influenced by the upwelling.

3.2. Description of molybdenum & vanadium distributions

Without salinity normalization, slightly elevated dMo was commonly seen in the upper 200 m water column west of 100°W (Fig. S1). After the dMo concentration was normalized to salinity 35 (dMo^n), the distribution was generally invarient across the EPZT (Fig. 2a), with an average dMo^n concentration of 108.2 ± 2.7 nmol/kg. However, a significant depletion of Mo in a few samples was observed within the ODZ and the hydrothermal plume (Fig. 2a).

As was mentioned earlier, in most of our dMo-depleted samples, the dMo^n concentration actually increased slowly over at least 19 months (Fig. 3). Indeed, only three samples in the section showed unchanging, low dMo^n. Those three unchanging samples were a) Stn. 2 at 3.5 m (dMo^n = 97.8 ± 0.7 nmol/kg), which was the station closest to the coast and the sample with the highest total Chl *a*; b) Stn. 6 at 125 m (dMo^n = 82.1 ± 2.0 nmol/kg), which was the depth of maxima in both nitrite (4.3 μmol/kg) and dissolved Mn (3.3 μmol/kg) for that station (though not for the entire ODZ); and, c) Stn. 20 at 2500 m (dMo^n = 94.2 ± 1.9 nmol/kg), which was the depth of the dissolved Mn maximum at this station and was immediately west of the crest of the EPR.

For the samples that did change with time, it would seem that Mo was slowly converted from a form not determined by our ICP-MS analysis back to molybdate. However, since the Mo ICP-MS analysis is a

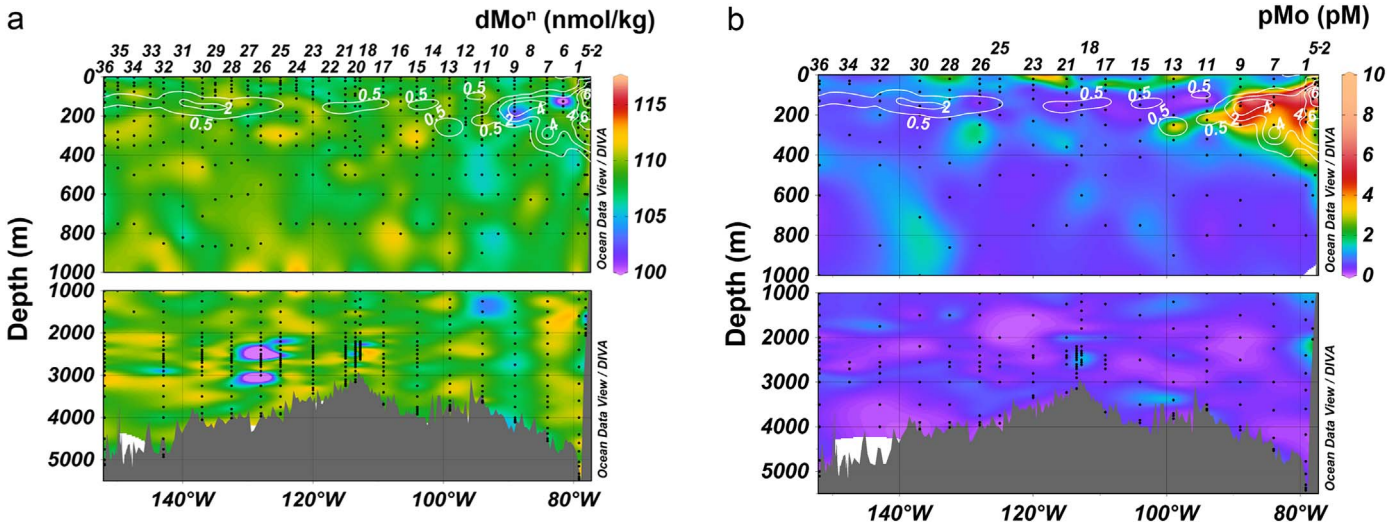

Fig. 2. (a) The distribution of dissolved Mo (normalized to salinity 35) along the EPZT. (b) The distribution of particulate (0.8–51 μm) Mo along the EPZT. In both graphs, white contours indicate dissolved nitrite concentration (μmol/kg).

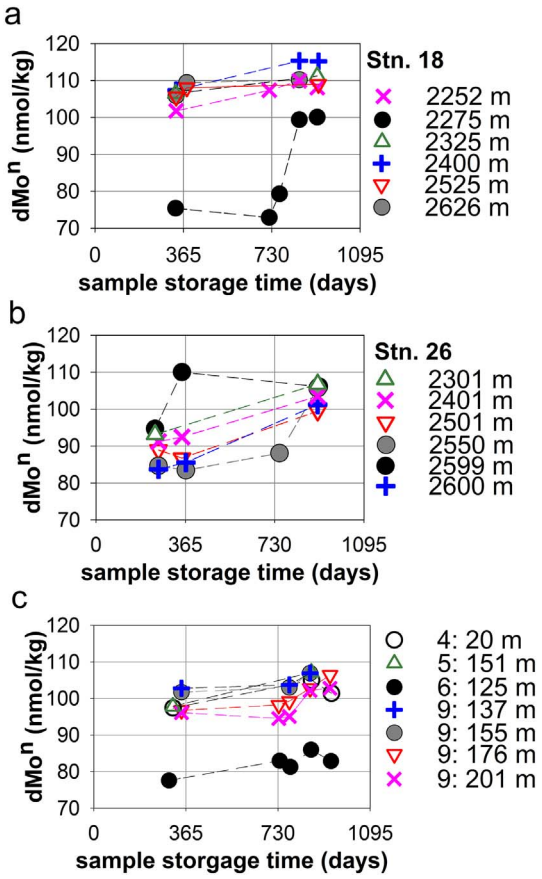

Fig. 3. Salinity-normalized dissolved Mo values as a function of sample storage times from (a) St.18, (b) St. 26, and (3c) the OMZ. Dashed lines show the trends of Mo increase with time.

"dilute-and-shoot" method that does not involve an extraction step, it seems unlikely that even a colloidal Mo species would be analytically invisible. We hypothesize that the missing Mo is in a form that was adsorbed to the sample container (acid-washed high-density polyethylene) walls even when the sample was acidified. For instance, Wang et al. (2009) developed a method in which what is thought to be Mo(V) is complexed with tartrate and extracted onto a non-ionic acrylic resin, thus suggesting that at least some organic Mo complexes might adsorb onto the walls of our sample containers. We are unaware of other reports of this sample storage phenomenon, though its transient nature might result in it being overlooked. Although we cannot explain this phenomenon, we infer that it represents a real change in Mo speciation since it was only observed in a limited number of samples and, as we shall show, those samples might reasonably be expected to have some change in Mo concentration or speciation. Therefore, we suggest that previous studies reporting conservative dMo behavior in other OMZs (Nameroff et al., 2002; Goswami et al., 2012) might have missed the observation of the unknown transient species depending on their sampling, sample processing, and analytical methods. Again, in our discussion here, we refer to all samples that showed either consistent or transient low dMo^n concentrations as being Mo-depleted.

Anomalously low dMo^n was observed in several parts of the section. In the upper part of the ODZ (Fig. 1b), low dMo^n was observed in several offshore samples in the secondary nitrite maximum (Stns. 6 and 9; Fig. 2a), including one sample mentioned above where the low dMo^n was not transient. Also, in some shallow (< 200 m) samples along the Peru margin (Stns. 1–5) depleted dMo^n (98.5–104.6 nmol/kg) was observed (Fig. 4a). Salinity normalized dMo was also significantly depleted (4–8 s.d.) in a number of samples in the general depth range of the hydrothermal plume (Fig. 2a). The magnitude of dMo^n depletion was higher off-axis (Stns. 25 and 26), compared with the depletion above the ridge crest (Stn. 18) (Fig. 2a).

The maximum pMo (16.8 ± 2.6 pmol/L at Stn. 4) in the section was observed in the ODZ (Fig. 2b). Particulate Mo data showed that most of the pMo (80–100%) was non-lithogenic across the EPZT (Figs. 2b and S2). Enriched pMo in the ODZ corresponded both with elevated nitrite concentrations (Fig. 2b) and with elevated particulate Fe (pFe) (Fig. S3).

The salinity-normalized dV^n EPZT section, which shows slight depletion in near surface waters and then relative constancy at depth (Fig. 5a), agrees with earlier observations in the open ocean (Collier, 1984; Jeandel et al., 1987; Middelburg et al., 1988). Without salinity normalization, the dV distribution shows the same basic trend (Fig. S4), though details are less clear. Previously reported average dV^n concentrations are 32.4 ± 2.7 and 32.0 ± 0.4 nmol/kg in Atlantic and Pacific surface water, respectively (Collier, 1984; Jeandel et al., 1987). In deep water, average dV^n appears to vary in different ocean basins (Atlantic Ocean: 32.0–35.3 nmol/kg; Pacific Ocean: 35.3 nmol/kg; Indian Ocean: 36.0 nmol/kg) (Collier, 1984; Middelburg et al., 1988), though intercalibration of these data sets is lacking. In our data, average dV^n was 32.6 ± 1.0 nmol/kg in the upper water column (< 450 m). Below 1000 m depth, average dV^n was 34.9 ± 1.8 nmol/kg.

As was the case with dMo^n, anomalously low dV^n (relative to the rest of the section) was found in several places in the EPZT. However, in contrast to dMo^n, depleted dV^n concentrations were stable; that is, they did not change with sample storage time. Low dV^n at Stn. 9 (~28.6 nmol/kg at 154 m) corresponded with the nitrite maximum (Fig. 5a). Here, the depletion of dMo^n and dV^n was mostly found in the same samples (Figs. 2a and 5a). This tends to confirm our observed Mo-depletion in the ODZ as more than simply an analytical artifact. Note that some other dissolved trace elements we determined in these samples (e.g., Ba, Ni) were not depleted; thus, the samples do not appear to be generally anomalous. Dissolved V depletion greater than the usual surface water depletion was also observed in near surface waters across the Peruvian continental shelf where dV^n concentrations ranged from 29.7–32.0 nmol/kg (Fig. 4b). The lowest dV^n in the coastal upwelling region was observed near the surface at Stn. 2 (the station closest to

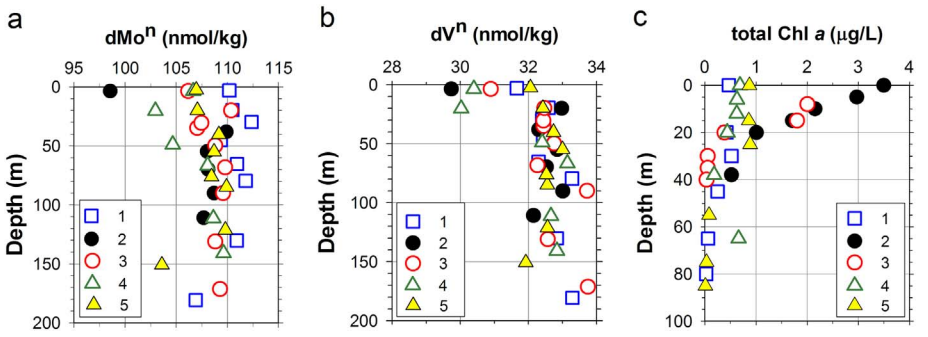

Fig. 4. The vertical distributions of (a) dissolved Mo (normalized to salinity 35), (b) dissolved V (normalized to salinity 35) and (c) total chlorophyll *a* in the upper 100 m on the Peru margin.

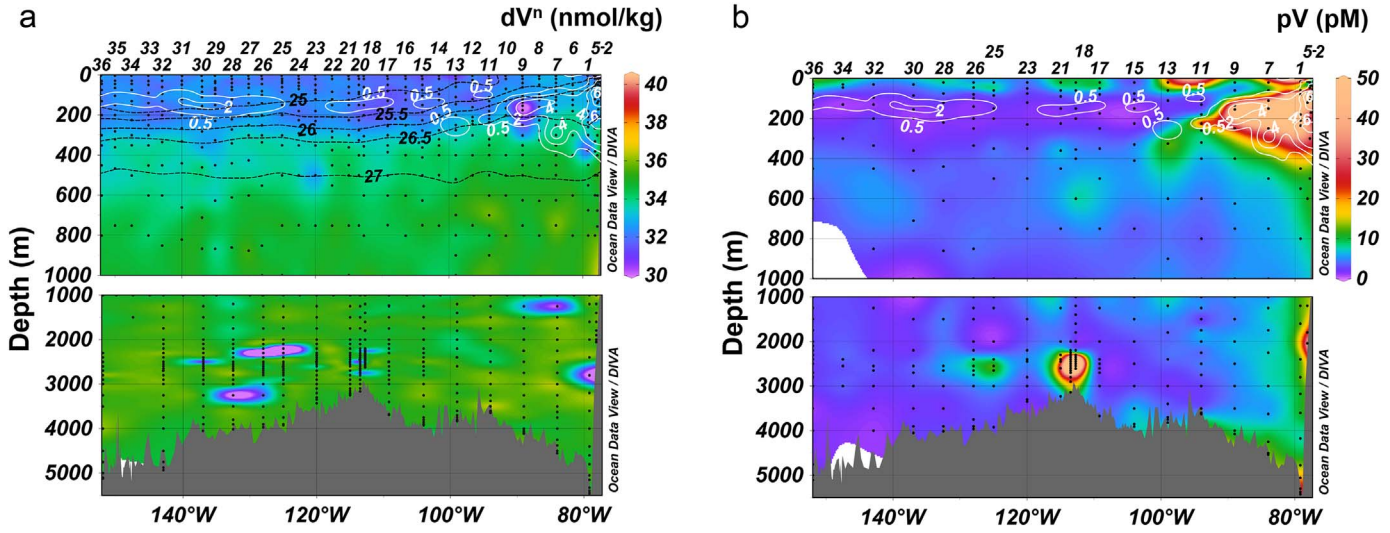

Fig. 5. (a) The distribution of dissolved V (normalized to salinity 35) along the EPZT. Black dashed lines indicate neutral density surfaces (25 kg $m^{-3} \leq \gamma^n \leq$ 27 kg m^{-3}). (b) The distribution of particulate (0.8–51 μm) V along the EPZT. In both graphs, white contours indicate dissolved nitrite concentration (μmol/kg).

shore), and also corresponded with the lowest dMo^n at the coastal stations (Fig. 4a and b). Depleted dV^n was also found in some samples in association with the hydrothermal plume (Fig. 5a). As with dMo^n, off-axis dV^n was more depleted (to as low as 17 nmol/kg at Stn. 26) than in the ridge crest (Stn. 18) samples. Additionally, a few V-depleted samples were found deeper in the water column (> 3000 m, Stns. 26 and 28) (Fig. 5a), along the boundary of elevated dissolved Fe in the off-axis hydrothermal plume (Resing et al., 2015).

In the particulate phase, elevated pV concentrations were seen in the ODZ and the hydrothermal plume. Non-lithogenic (average 92%) pV was dominant across the EPZT (Figs. 5b and S5). This pV behavior is similar to that of pMo, discussed above. West of Stn. 13, pV additionally shows an enrichment in the mixed layer and then a slight minimum in the 100–300 m depth range coincident with the nitrite maximum and where suspended particulate matter concentrations typically decrease and the nutricline begins. The mixed layer pV enrichment is reflected both in the small and large particulate fractions and, in contrast to most of the rest of the section, large particulate V is generally the dominant pV mixed layer fraction, averaging 59% of the total. Lee et al. (2017) attributed the elevated large pV concentrations in the mixed layer to V uptake by diatoms, as evidenced by the fact that biogenic Si is the only carrier phase similarly showing elevated large particulate fractions in the mixed layer (Lam et al., 2017). The slight pV minimum below the mixed layer (where the small particulate fraction dominates), however, is due solely to changes in the small particulate fraction. Close to the Peru margin, upper water column pV concentrations are generally higher than further west and the pV minimum is no longer apparent.

3.3. Molybdenum and vanadium behavior in the hydrothermal plume

The depletions in dMo^n and dV^n in the hydrothermal plume are both apparent in our sections (Figs. 2a and 5a) and, as we shall show, puzzling aspects of our distributions. At the ridge crest (Stns. 18 and 20), these depletions in dV^n and dMo^n corresponded to enrichments in pV and pMo associated with pFe enrichments (Fig. 6) while off-axis (Stns. 26 and 28) larger patches of dV^n and dMo^n depletion are observed toward the boundaries of pFe-enriched waters (purple patches in Figs. 2a and 5a). We note that Mo and V were analyzed by different methods and that other elements analyzed at the same time (e.g., Ba with Mo; Ni with V) showed no anomalous behavior. Thus, we view these dMo^n and dV^n depletions as being robust and not indicative of generally anomalous samples. Because no significant sulfide was observed in the water (< 60 pM; Cutter et al., 2017) or in the hydrothermal particles (Hoffman et al., 2017), formation of thiomolybdate or particulate sulfides seem unlikely factors in the Mo and V removal. Adsorption of these elements onto hydrothermal Fe and Mn oxides is thus the most likely possibility for removal of these elements (e.g, Trefry and Metz, 1989; Kashiwabara et al., 2011) and we explore this further with the particulate data.

We initially confine our consideration of hydrothermal oxide scavenging of Mo and V to waters 2300 m and deeper at Stns. 18 and 20, i.e., waters at the ridge crest with pFe concentrations > 1 nM. Since pFe was typically 10-fold greater in concentration than particulate Mn (pMn), it is tempting to focus just on pFe as the adsorbing phase. Note, however, that there is evidence that δ-MnO_2 more strongly adsorbs Mo than Fe oxyhydroxides (e.g., Kashiwabara et al., 2011). Based on pAl

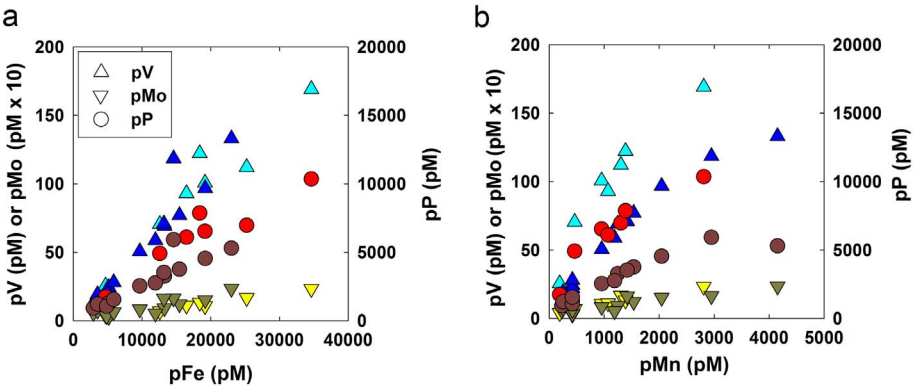

Fig. 6. The relationships between small fraction (0.8–51 μm) particulate elements (V: light blue at Stn.18/ dark blue at Stn. 20; Mo: yellow at Stn. 18/green-grey at Stn. 20; P: red at Stn. 18/brown at Stn. 20) and (a) particulate Fe/ (b) particulate Mn in the ridge-crest plumes. (For interpretation of the references to colour in this figure legend, the reader is referred to the web version of this article.)

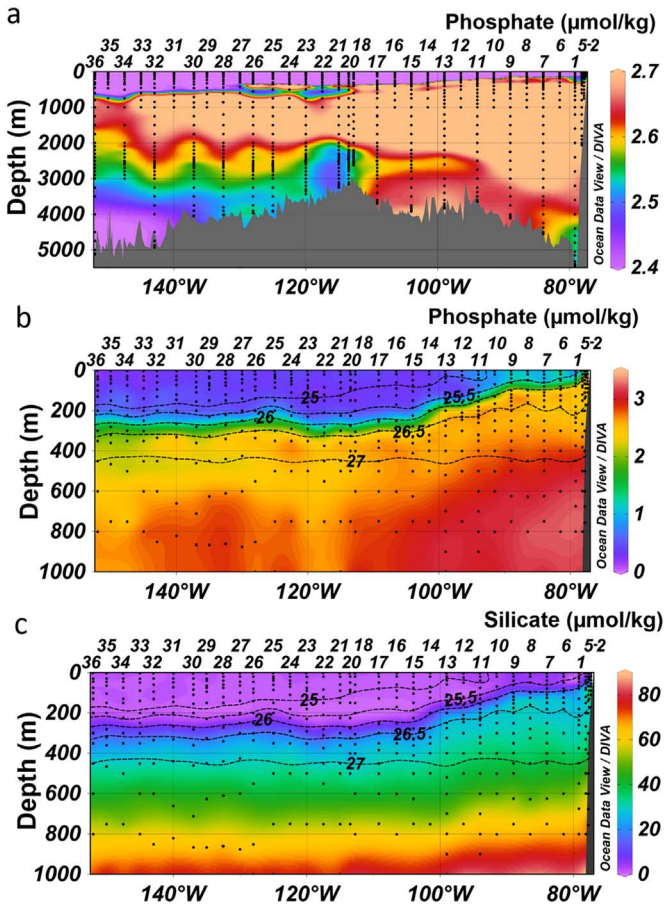

Fig. 7. (a) The distribution of dissolved phosphate along the EPZT. Note expanded concentration scale which emphasizes the range of concentrations associated with waters affected by the hydrothermal plume. The distributions of (b) phosphate and (c) silicate (μmol/kg) in the upper 1000 m of the water column along the EPZT. Black dashed contours indicate neutral density surfaces (25 kg $m^{-3} \leq \gamma^n \leq$ 27 kg m^{-3}).

concentrations, lithogenic pMo, pV, pMn, and pFe were generally < 1% of the total particulate concentrations in these hydrothermally-influenced waters (Lam et al., 2017) and are thus ignored. Fig. 6 shows that in the small particulate fraction both pV and pMo are significantly correlated with both pFe and pMn in the ridge crest plume. Note that the concentrations of the large particulate V were also greatly increased in the ridge crest plume (Stns. 18 and 20), even though the small fraction was still the majority of the total particulate concentrations. The large particulate pV/pFe ratio in these plume samples was statistically the same as the small particulate ratio. Lee et al. (2017) noted that hydrothermal pFe and pMn at Stns. 18 and 20 show different size partitioning, with pFe mostly (~80%) occurring in the small particulate fraction, while pMn occurring almost evenly between small and large particulate fractions. Interestingly, the fractions of total pV and total pFe of these hydrothermal samples that were in the large size particles were similar (median 27% and 24%, respectively; Fig. S6). In contrast, the fraction of total pMo of these samples that was in the large size particles (median 34%; Fig. S6) was midway between the large fraction percentages for pFe and pMn (median 24% and 49%, respectively; Fig. S6). These observations are compatible with pFe being the main scavenger for pV while pMo may well be scavenged by both pFe and pMn.

Using an estimated global hydrothermal Fe input of ~10 Tg/yr (Poulton and Raiswell, 2002) and assuming most of this Fe precipitates and is removed to the sediments, then the EPZT hydrothermal pMo/pFe molar ratio of 6.4×10^{-5}, yields a Mo removal rate of $\sim 10^7$ mol/yr or ~5–10% of the estimated fluvial dissolved Mo flux (Gaillardet et al., 2014). Similarly, the EPZT hydrothermal pV/pFe molar ratio of 5.1×10^{-3}, yields a V removal rate of $\sim 10^9$ mol/yr or about twice the estimated fluvial dissolved V flux (Gaillardet et al., 2014). Similar calculations can be made using the estimated 1–2 $\times 10^{10}$ mol/yr global accumulation of Mn in metalliferous sediments (Elderfield and Schultz, 1996) and these yield similar results for hydrothermal Mo and V removal. While there is considerable uncertainty in all of the numbers used for these estimates, the results are nonetheless in general accord with the conclusion of Trefry and Metz (1989) who suggested that adsorption onto hydrothermal precipitates was a major mechanism of removal of dV from the ocean as well as the similar conclusion for dMo removal (Kashiwabara et al., 2011 and references therein).

In order to understand whether hydrothermal pFe adsorption of V (and possibly Mo) should affect their dissolved distributions, we next consider phosphate, which has previously been shown to be adsorbed onto hydrothermal pFe (e.g., Wheat et al., 1996; Feely et al., 1998). Close inspection of the dissolved phosphate distribution in the hydrothermal plume (Fig. 7a) suggests adsorptive removal of ~100–150 nM PO_4^{3-} in the most pFe-rich waters at Stns. 18 and 20. For the particulate phosphorus (pP) in the hydrothermal plume, lithogenic corrections are again trivial and ignored. Also, assuming a C/P Redfield Ratio of 117, the POC data suggests that biological contributions to pP in the hydrothermal plume are likewise trivial (i.e., the median POC/pP molar ratio in the plume waters is 10) (Lam et al., 2017). The hydrothermal pP-pFe relationship (Fig. 6) shows a good correlation and indicates a pP/pFe molar ratio of 0.29, which is about 50% higher than the P/Fe ratio Ohnemus et al. (2017) estimated for EPZT hydrothermal particles from particles filtered from GoFlo bottles. Taking the 100–150 nM estimate of hydrothermal PO_4^{3-} adsorptive removal and the hydrothermal pV/pP molar ratio (0.016), thus suggests we should expect a 2–3 nM dV removal onto hydrothermal pFe. For Mo, the pMo/pP molar ratio (1.8×10^{-4}) indicates an insignificant dMo removal of only a few pM. These crude calculations indicate that we might see some dV removal at the ridge crest but not in the extended plume and we should not see any dMo removal. This conclusion is clearly at odds with our observations and indicates that something else must be responsible for the significant dMo^n and dV^n depletions at Stns. 26 and 28.

We briefly consider several other possibilities for the hydrothermal dissolved Mo and V removal. First, more depleted dMo^n and dV^n in the off-axis plume than in the ridge-crest plume might be a result of different hydrothermal sources in the off-axis plumes (Stns. 25 and 26) from the ridge-crest plumes (Stns. 18–21), as evidenced by the ^{228}Ra measurements in hydrothermal plume waters (e.g., Stn. 20: 3.2–5.5 yr; Stn. 25: 2.7–5.4 yr old) (Kipp et al., 2017). Likewise, Resing et al. (2015) suggested that off-axis hydrothermal samples (Stns. 20–36) were derived from vent fields south (~17°S–18.5°S) of the EPZT section while anomalously low excess ^3He at Stn. 18 was likely a signal from local hydrothermal activity (Jenkins et al., 2017). Certainly, this observation is not surprising since various hydrothermal vent sites are distributed along the EPR and the EPR plumes are not restricted to the axial valley (German and Von Damm, 2006; Wu et al., 2011; Resing et al., 2015). Thus, the different extent of dMo^n and dV^n depletion between the ridge-crest plume and the off-axis plume may well reflect different vent sources. In contrast, the ^3He data (Jenkins et al., 2017) and positive linear correlations between excess ^3He with dissolved Fe and dissolved Mn from the first off-axis station (Stn. 20) of the EPR to the westernmost station (Stn. 36) (Resing et al., 2015) indicate that the off-axis samples form a continuous plume. However, the locale of additional hydrothermal sources across the EPZT suggested by the ^{228}Ra data (Kipp et al., 2017) is incompatible with that suggested by other data (^3He, dissolved Fe and dissolved Mn; Resing et al., 2015). Thus, the extent to which the extended hydrothermal plume observed during the EPZT reflects one or many sources is unresolved.

A change in competition for adsorption sites due to concentration changes in another element is another possible explanation for our observations that seems unlikely. Phosphate is likely the highest concentration strongly competing element (Feely et al., 1998; Brinza et al.,

2008) and its dissolved concentration varies minimally and, in fact, increases slightly off-axis (Fig. 7a) where we see the highest dMo^n and dV^n removal.

Alteration of the structure of hydrothermal particles during off-axis transport (Fitzsimmons et al., 2017) and thus alteration of their adsorption capacity is another possibility. Indeed, at the ultramafic-hosted Rainbow hydrothermal site on the Mid-Atlantic Ridge, Edmonds and German (2004) did observe progressive increases in particulate V/Fe ratios going from young buoyant plumes to neutrally buoyant plumes, and ultimately to the highest V/Fe ratios in the underlying hydrothermal sediments. Likewise, Brinza et al. (2015) found that as ferrihydrite ages to hematite, sorbed V and Mo become incorporated into the hematite structure while Kashiwabara et al. (2011) found that molybdate adsorbs to ferrihydrite as an outer sphere complex but to hematite and goethite as an inner sphere complex. These observations and experiments are thus compatible with increased removal of V and Mo from the water with plume particle age. We note that from ^{228}Ra measurements in the EPZT hydrothermal plume samples, Kipp et al. (2017) estimated a significantly greater age for samples at Stn. 20 (2.4–5.5 yrs) than for the axial Stn. 18 (~1 mo.).

Since pV in the EPZT extended hydrothermal plume was significantly greater than the deep water background concentrations, we can at least partially test this idea. If we confine our analysis to hydrothermally-influenced samples with pV > 9 pM (i.e., about 3× greater than the pelagic deep water background in the EPZT of 2–4 pM), then non-lithogenic pV/pFe molar ratios cluster around $5.3 \pm 0.8 \times 10^{-3}$ and show no relationship with distance from the ridge crest (Fig. S7). Thus, this provides no evidence of significantly changing pV/pFe with particle ageing. Interestingly, the one dV-depleted plume sample where we have both dissolved and particulate data (Stn. 20, 2500 m, dV^n = 19 nmol/kg) had the highest non-lithogenic pV/pFe molar ratio (8.1×10^{-3}) of these samples. This is, of course, scant evidence on which to build a hypothesis as well as only a relatively modest pV enrichment. In any event, we find no support for large changes in V adsorption in the EPZT hydrothermal particle data. Given that the hydrothermal dV^n depletions are at the edges of the pFe plume, we can only speculate that breakdown of the organic matrix associated with hydrothermal pFe (Fitzsimmons et al., 2017) might result in more exposed pFe surface area and ultimately aggregation and removal by sinking.

3.4. Molybdenum and vanadium in shallow waters

Through most of the section, the transition from slightly dV-depleted shallow waters to higher dV^n deep waters occurs in the neutral density range γ^n = 25.5–26.5 kg/m^3 which is also where the sharpest gradients in phosphate and silica concentrations occur (Fig. 7b,c). Enrichment of pV in surface waters with dominance in the large particulate fraction suggests that V was taken up by biogenic particles (likely diatom) (Lam et al., 2017; Lee et al., 2017; Osterholz et al., 2014), which is compatible with the observation of surface water dV^n depletion. Our observations thus suggest that the dV^n gradient in the water column (200–400 m) in the pelagic region is mostly controlled by shallow biological removal and deeper regeneration.

Near the Peru margin, nutrient gradients still follow the density gradient; however, the relationship between dV^n and density weakens (Fig. 5a), suggesting additional processes influencing the dV^n distribution in this environment. Given the removal of dV in hypoxic Louisiana Shelf waters (Shiller and Mao, 1999) and the slight Mo depletion in those same waters (Joung and Shiller, 2016) as well as the low oxygen water impinging on the Peru margin in the EPZT, we more closely examined our dMo^n and dV^n profiles across that margin (Stns. 1–5; Fig. 4). We do indeed observe some shallow (< 200 m) samples with depleted dMo^n (98.5–104.6 nmol/kg). Again, those samples with slightly or moderately depleted Mo (1.5–4 s.d.) were reanalyzed to validate the depletion. We do not see high nitrite or dissolved/particulate Fe or Mn in these Mo-depleted samples relative to other shallow samples in the margin stations. Thus, there is no evidence of a recent, substantially different, impact of scavenging, denitrification, or sediment interaction.

Similar to our observations of Mo, dV^n depletion greater than the usual surface water depletion was observed in near surface (< 50 m) waters of Stns. 1–5 across the Peruvian continental shelf where concentrations ranged from 29.7–32.0 nmol/kg. The lowest dV^n in the coastal upwelling region was observed near the surface at Stn. 2 (the station closest to shore), and also corresponded with the lowest dMo^n and the highest total Chl *a* in the coastal stations (Fig. 4). Other dV^n- and dMo^n-depleted samples in this part of the section were also generally in the shallowest waters of the three most inshore stations. Given that dMo and dV were analyzed by different methods at different times, we view this as a robust observation, despite the concentration changes being close to our analytical precision. Since nearshore pFe enrichment was coincident with the high nitrite plume below 100 m (i.e., well below where we observe shallow dV^n and dMo^n depletion), adsorptive removal or removal associated with denitrification seems unlikely. However, apparent biological uptake of Mo from surface waters has been reported by Wang et al. (2016) who observed non-conservative dMo behavior in the Taiwan Strait. Likewise, Osterholz et al. (2014) observed significant dV removal in diatom cultures. Surface waters of the inshore EPZT stations had the greatest amount total Chl *a* and the protective pigments diadinoxanthin, diatoxanthin, and β-carotene of the entire section (Moffett et al., 2015) as well as the highest amount of opal (Lam et al., 2017). Taken together, our observations thus suggest biological uptake and/or adsorption onto organic particles as the likely cause of the shallow inshore dV^n and dMo^n depletions in the EPZT section.

The V section also allows us to revisit the issue of whether coastal shelf redox processes play a significant role in overall surface ocean V depletion as suggested by Shiller and Mao (1999). We do note that the expansion of the upper ocean dV^n depleted depth range east of Stn. 13 (99°W) may relate to both biological and redox processes (see next section). However, the pelagic vertical dV^n gradient still tends to follow the nutricline and thus occurs slightly shallower than might be expected from the OMZ dV depletion along the margin. In contrast to the Louisiana Shelf observations (Shiller and Mao, 1999; Joung and Shiller, 2016), we did not observe dV^n (or dMo^n) depletions in oxygen-depleted bottom waters on the Peru margin. Also, there was no significant horizontal gradient in upper water dV^n depletion away from the margin as would be expected if margin processes dominated shallow V removal. Thus, the EPZT data seem to argue against a large redox effect on the pelagic dV distribution. Nonetheless, we cannot rule out a margin effect elsewhere in the ocean where, for example, an extreme oxygen minimum intersects a wider margin than occurs off the west coast of Peru.

3.5. Mo and V behavior in the offshore ODZ

As noted above, significant dV^n and dMo^n depletion was observed in a few samples in the offshore ODZ (Figs. 2a and 5a). This is especially apparent at Stn. 9 where several samples in the 150–200 m depth range are depleted in both elements and which corresponds to a pool of water with high nitrite as well as high I^- and low IO_3^- (Cutter et al., 2017), high dissolved and labile Co (Hawco et al., 2016) and elevated pFe (Heller et al., 2017). That said, there is higher nitrite water (also with high I^- and low IO_3^- as well as high Co and high pFe; Cutter et al., 2017; Hawco et al., 2016; Heller et al., 2017) close to the coast at Stns. 2–5 which does not show significant dMo^n depletion and which has a dV^n depletion similar to the typical upper water column depletion.

No significant dissolved sulfide was observed in these Mo and V depleted waters (Cutter et al., 2017) and only low pM amounts of acid volatile sulfides were detected (Ohnemus et al., 2017). Thus, formation of thiomolybdate or particulate sulfides seem unlikely factors in the Mo and V removal. Likewise, Scholz et al. (2017) summarize observations

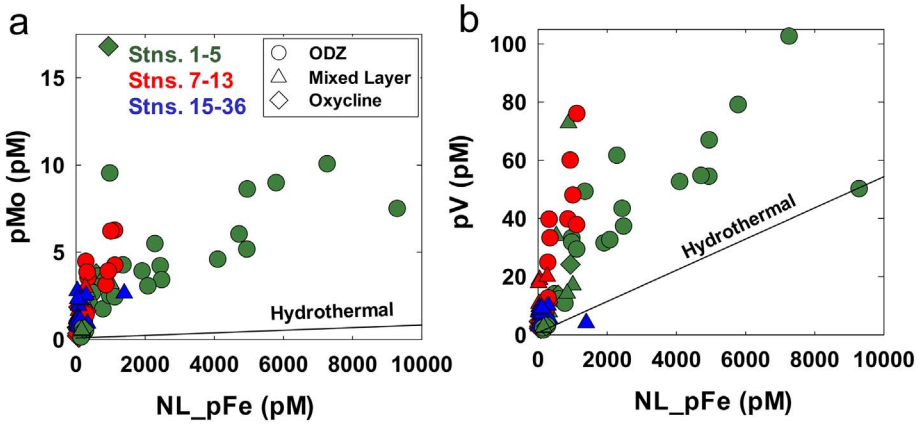

Fig. 8. The relationships of small (0.8–51 μm) (a) particulate Mo and (left)/ (b) particulate V (right) with and non-lithogenic Fe in the upper 500 m of the water column along the EPZT. For clarity, only ODZ, mixed layer and upper oxycline samples in the upper 500 m are shown here.

for this region and discount sulfide as a factor in Mo cycling. Recent work suggests two other possible processes that might explain the dMo and dV depletions. Scholz et al. (2011, 2017; see also Heller et al., 2017) proposed that Fe oxides that are reductively dissolved in the anoxic benthic boundary layer re-precipitate at the oxycline or below to scavenge Mo and V and then ultimately settle to the sediments for burial at the boundaries of the ODZ. Since the Fe can cycle through this process repeatedly, Fe oxides can be viewed as shuttling the Mo and V to the sediments. An alternative mechanism, discussed by Ohnemus et al. (2017) using other EPZT data, involves denitrifying prokaryotes taking up various trace elements, including V, in the ODZ. This is also consistent with the utilization of Mo in bacterial nitrate reductase (Tsementzi et al., 2016). For V, there are some reports of nitrate reductases that lack Mo and contain V instead (Rehder, 2008 and references therein), though the presence of V nitrate reductase in the ocean is, as yet, unknown.

Confounding any attempt to deconvolve the effects of redox shuttling versus heterotrophic uptake on Mo and V cycling in the ODZ is the fact, noted by Ohnemus et al. (2017), that pFe is enriched in ODZ waters roughly coincident with the enrichment in nitrite. Indeed, Heller et al. (2017) observed oxidation of dissolved Fe(II) to particulate Fe(III) in the upper ODZ of the EPZT section. Heller et al. (2017) and Scholz et al. (2016) further suggested coupling between the Fe and N redox cycles. To help resolve this overlap of processes, we examine the particulate data to see if it might shed further light on ODZ Mo and V cycling. We note that the pump particles considered here include pMo and particulate organic carbon (POC) data that were not available to Ohnemus et al. (2017) in their consideration of bottle particulates in the EPZT.

We first plot pMo and pV versus the non-lithogenic pFe in ODZ, upper oxycline, and mixed layer samples from the upper 500 m of Stns. 1–36 (Fig. 8). If we compare element-Fe relationships in the ODZ with those same relationships for ridge crest particles under the assumption that adsorption onto Fe oxyhydroxides controls pMo and pV concentrations in both regions, then inshore ODZ Fe particles (Stns. 1–5; green circles in Fig. 8) would need to sorb > 10 × more Mo per mole of pFe and 3 × more V than hydrothermal pFe. For the offshore ODZ (Stns 7–13; red circles in Fig. 8), Fe precipitates would need to sorb ~80 × more Mo and > 10 × more V per mole pFe than hydrothermal precipitates. Certainly, adsorption capacities of Fe oxyhydroxides can vary substantially and are likely to be affected by pH, organic matter, and competing ions. Additionally, evidence suggests that the precipitation of ODZ Fe oxyhydroxides occurs in the absence of dissolved oxygen (Scholz et al., 2016; Heller et al., 2017), which is not likely the case for ridge crest precipitates, which may result in different scavenging characteristics for these oxyhydroxides. Indeed, Heller et al. (2017) reported at least some lepidocrocite in the ODZ while Hoffman et al. (2017) found ferrihydrite-like oxyhydroxides in the hydrothermal plume of the EPZT section. This mineralogical difference could also contribute to differences in scavenging removal by pFe in the ODZ versus the hydrothermal plume (e.g., Kashiwabara et al., 2011). Thus, using ridge crest precipitate composition to correct for Fe oxyhydroxide adsorption onto ODZ Fe precipitates is potentially problematic (Ohnemus et al., 2017). Furthermore, while the pMn concentration was typically < 1% that of pFe in the upper ODZ, above the ridge crest pMn was typically 8% of pFe concentration. As was discussed in the hydrothermal section, above, particulate MnO_2 may well be an important or even dominant Mo adsorbing phase above the ridge crest, complicating the application of hydrothermal element-Fe relationships to the ODZ. Thus, compositionally, it is difficult to rule out adsorption onto Fe precipitates as a significant factor affecting Mo and V in the ODZ.

Fig. 9 shows pMo and pV plotted versus POC (Lam et al., 2017) for small particulate fraction samples in the ODZ, upper oxycline above the ODZ, and the mixed layer throughout the transect. Plotting versus particulate nitrogen or phosphorus shows similar trends. Corrections for lithogenic contributions are minor, typically 3% of pV and < 1% for

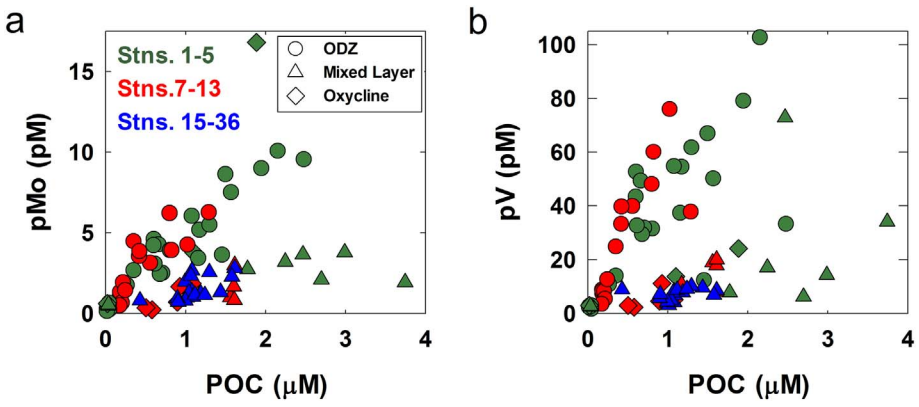

Fig. 9. The relationships of small (0.8–51 μm) (a) particulate Mo and (b) particulate V with POC in the upper 500 m of the water column along the EPZT. For clarity, only ODZ, mixed layer and upper oxycline samples in the upper 500 m are shown here.

pMo, and were not made to the data. For Mo, the Fe correction based on the hydrothermal pMo-pFe relationship affects pMo concentrations in the ODZ, oxycline and mixed layer trivially, typically only 2%. For pV, the Fe correction is larger, typically 21%; however, making the correction does not change the trends in Fig. 9. Because of the trivial nature of the lithogenic correction and the uncertain nature of the Fe adsorption correction (which is small if we use hydrothermal element-Fe relationships), we therefore show the original, uncorrected data. For pV, our results are in general agreement with those of Ohnemus et al. (2017). That is, ODZ particles are clearly enriched in pV relative to the mixed layer and oxycline and there is a general trend of increasing pV with POC. Similar trends are also observed for pMo. Thus, the ODZ cycling of V and Mo could well involve biotic incorporation into organic matter and/or removal by adsorption onto organic particles.

Scant data on cellular V and Mo quotas is available to test this idea that the ODZ pV and pMo enrichments are biogenic. Much of the available data for Mo and V relates to diazotrophs and not to the heterotrophic prokaryotic community of the ODZ. In an N_2-fixing soil bacterial mutant that expresses only V-nitrogenase, Bellenger et al. (2008) found cellular V/P molar ratios of $\sim 1.5 \times 10^{-4}$ at seawater concentrations of dV. Tovar-Sanchez and Sañudo-Wilhelmy (2011) measured metal:P cellular quotas in *Trichodesmium* colonies in subtropical Atlantic waters influenced by the Amazon plume and found V/P molar ratios of 5–11 $\times 10^{-3}$ and Mo/P molar ratios of 1–10 $\times 10^{-3}$. Osterholz et al. (2014) reported cellular V/P molar ratios of 4–11 $\times 10^{-3}$ for two diatom cultures. Ho et al. (2003) suggested an average oceanic phytoplankton Mo/P molar ratio of 3×10^{-5}. Tuit et al. (2004) examined Mo quotas in two N_2-fixing cyanobacteria and reported Mo/C molar ratios of $0.7 \pm 0.3 \times 10^{-6}$. For the EPZT ODZ samples, Ohnemus et al. (2017) estimated a V/P molar ratio of 3×10^{-3} and our data indicate molar ratios of V/P = 4×10^{-3}, Mo/P = 5×10^{-4}, and Mo/POC = 5×10^{-6}. Thus, while the available biological data are scattered and not necessarily applicable to the relevant ODZ biota, they nonetheless indicate that the necessary cellular element ratios are within reasonable biological possibility. However, seeing that particulate metal/C ratios in ODZ waters are higher than in the mixed layer (Fig. 9) does require significantly increased metal quotas for the ODZ heterotrophic biota as compared with mixed layer phytoplankton, as was noted by Ohnemus et al. (2017).

Note that inclusion of the large particulate fraction in this discussion does not significantly alter our conclusions. While the large size pV in the oxycline often was greater than small pV (presumably because the oxycline is shallow and receives large size pV from the mixed layer), large pV was generally less than a third of the total pV in the ODZ. More details of processes controlling pV size partitioning in the ODZ are discussed by Lee et al. (2017). However, for the inshore stations (Stns. 1–5), the pV/POC ratios were typically 3 times higher in the large particles than the small. Furthermore, there was no clear correlation in the large fraction between pV and POC across the ODZ. These observations make sense both in the context of heterotrophic metal uptake more likely involving small (i.e., < 51 μm) cells thereby leading to a lack of pV-POC relationship in large particles as well as small FeOOH precipitates aggregating to form larger particles leading to a similar pV-pFe relationship in small and large particles.

Despite the fact that there are potential mechanisms for removing dMo and dV, we note that the highest ODZ pV and pMo concentrations are found at the most inshore stations. Indeed, that is where the Fe oxide shuttling mechanism is most likely to be relevant (Scholz et al., 2011, 2017). Thus, we are still left with the puzzle of why we don't see even greater dissolved phase Mo and V depletions nearshore than offshore at Stn 9. We note, however, a slight upward doming of isopycnals in the upper few hundred meters at Stn. 9 (Fig. 5a) which is possibly indicative of a cyclonic eddy. Eddies can be important in offshore transport of waters along eastern upwelling margins (Pegliasco et al., 2015). Although the sampling period of the cruise was during the annual minimum of eddy activity along the Peruvian coast (Chaigneau et al., 2008), the occurrence of an eddy is still possible and supported by a relatively weak seasonal variation (~10%) of the surface eddy kinetic energy observed around 10°S off the Peru coast (Colas et al., 2012). Additionally, subsurface anticyclonic eddies generated at the bottom boundary layer of the continental slope in the Peru-Chile Undercurrent can transport low oxygen and elevated nitrite waters offshore (Thomsen et al., 2016). Because of persistent cloud cover during the EPZT transect, daily satellite imagery is not available. However, monthly composites for November 2013 (Fig. S8) show dynamic features in the chlorophyll imagery trending southwestward away from the coast as well as a surface temperature front where the Peru Coastal Current likely bifurcates (Penven et al., 2005). Thus, the cruise track passed through a clearly dynamic region and the waters at Stn. 9 may well have come from the northeast where the shelf is somewhat broader and the ODZ also extends further offshore. This may well explain the discontinuous nature of nitrite and some other chemical distributions and suggests the offshore ODZ dMo and dV depletions are remnant signals of more intense removal near the coast.

4. Conclusions

Our presentation of the first detailed oceanic sections of dissolved Mo and V largely confirms past interpretations of the distributions of these two elements (Morris, 1975; Collier, 1984, 1985; Middelburg et al., 1988; Sherrell and Boyle, 1988; Tuit, 2003). In the broad picture, Mo behaves conservatively while V is nearly so, with only a ~5% increase in concentration with depth. However, some interesting details emerge from the sections.

For dissolved Mo, a small number of samples showed significantly depleted concentrations which, in most cases, gradually increased with time. We hypothesize that the original sample had experienced a change in speciation of dissolved Mo from the predominant molybdate to another, as yet, unknown form. Because these Mo depletions were not randomly scattered but instead corresponded with other factors including low oxygen, high nitrite, depleted V, and/or the hydrothermal plume, along with the observation of pMo and pV enrichments in the OMZ and the hydrothermal plume, these Mo depletions (or speciation changes) cannot be dismissed as random analytical artifacts. However, full understanding or exploitation of this information necessarily awaits further analytical development. Note that due to lack of observable sulfide in the section, formation of thiomolybdates is probably not a factor.

For dissolved V, the transition from slightly V-depleted surface waters to slightly V-enriched deeper waters generally occurs in the same density range as the most rapid increase in nutrients. Closer to the Peru margin, this relationship between the V gradient, pycnocline and nutricline is less clear. Depleted dV^n (and dMo^n) were found in a few samples within the ODZ, generally associated with the nitrite maximum. Increased non-lithogenic pV (and pMo) were also observed in these upper ODZ waters and correlated with pFe. These results, along with the reported oxidation of dFe(II) to pFe(III) in the upper ODZ of the EPZT section (Heller et al., 2017), are supportive of the mechanism proposed by Scholz et al. (2011) for the adsorption of these oxyanions onto reprecipitated Fe (oxy)hydroixdes in the upper ODZ resulting in a shuttling of V and Mo to the sediment surface. There may also be some additional dV and dMo removal in the ODZ due to biological uptake, presumably in association with nitrogen cycling (Crans et al., 2004; Maia et al., 2017). This is supported both by correlations between POC and pV or pMo as well as reasonable requirements for V and Mo biological uptake.

Particulate Mo and V are mostly found in non-lithogenic phases across the section. Enriched pMo and pV in the ODZ were well-correlated with both pFe and POC and found in association with the nitrite maximum, which implies that Mo and V in the ODZ are likely scavenged by Fe (oxy)hydroixdes as well as taken up by the biota. Slightly increased pMo was seen in the ridge-crest plume near the EPR while

elevated pV was observed in both the ridge-crest plume and the off-axis plume. Both pMo and pV were well correlated with pFe and pMn in the hydrothermal plume, suggesting the scavenging removal of Mo and V onto hydrothermal Fe/Mn (oxy)hydroxide precipitates.

Additional slight depletions of dV^n and dMo^n in nearshore surface waters, relative to offshore surface water, and coincident with higher total Chl *a* concentrations toward the Peruvian coast, suggests removal by biological activity. Due to the absence of low V and/or Mo in the shelf bottom waters, the removal of these elements to anoxic sediments did not appear to be significant, at least in this section. Thus, our data do not support the proposal that incorporation of V into reducing shelf sediments contributes to the overall oceanic shallow water dV depletion (Shiller and Mao, 1999).

Depleted dV^n and dMo^n were also seen in association with the hydrothermal plume emanating from the EPR. Non-lithogenic pV and pMo correlated with pFe in plume waters and suggests adsorption onto hydrothermal Fe oxyhydroxides are a dominant oceanic sink for V and a minor one for Mo, in agreement with previous observations (e.g., Trefry and Metz, 1989). Greater depletion of the dissolved concentrations of these elements in some off-axis samples than in ridge crest samples as well as in samples from the plume margins remains an enigma, possibly relating to different hydrothermal vent sources, particle ageing, or breakdown of hydrothermal plume particles increasing the scavenging of these two oxyanions.

While the sections presented here do not substantially change our picture of the distributions of dissolved V and Mo in the ocean, they do provide constraints on these elements' cycles and provide guidance for future work. In particular, highly reducing environments, not considered in this section, remain important regions for the removal of V and Mo. Further development of methods for determining the speciation of these elements as well as more detailed studies of shelf and hydrothermal regions will likely improve our understanding of the oceanic cycling of V and Mo as well as potentially provide improved insight into their roles in biological and redox cycles.

Supplementary data to this article can be found online at https://doi.org/10.1016/j.marchem.2017.12.003.

Acknowledgements

We thank Jim Moffett and Greg Cutter for their successful leadership role of this expedition. This work was significantly aided by the skilled, hardworking supertechs, the staff of the Oceanic Data Facility, and the Captain and crew of the Thomas G. Thompson. We especially thank Missy Gilbert for her analytical skills in our lab and Daniel C. Ohnemus and the pump team for particle collection at sea. We thank Inia Soto Ramos for providing the supplementary satellite imagery. Review comments on an initial version of the manuscript resulted in significant improvement of this work. This work was funded through National Science Foundation grant OCE-1261214 to AMS and OCE-1518110 to PJL. Data produced under this grant have been submitted to BCO-DMO and accepted as intercalibrated by the GEOTRACES Standards and Intercalibration Committee.

References

Anbar, A.D., 2004. Molybdenum stable isotopes: observations, interpretations and directions. Rev. Miner. Geochem. 55, 429–454.

Antipov, A.N., Lyalikova, N.N., Khijniak, T.V., L'Vov, N.P., 1998. Molybdenum-free nitrate reductases from vanadate-reducing bacteria. FEBS Lett. 441 (2), 257–260. http://dx.doi.org/10.1016/S0014-5793(98)01510-5.

Baes, C.F., Mesmer, R.E., 1976. The Hydrolysis of Cations. Wiley, New York.

Bellenger, J.P., Wichard, T., Kraepiel, A.M.L., 2008. Vanadium requirements and uptake kinetics in the dinitrogen-fixing bacterium *Azotobacter vinelandii*. Appl. Environ. Microbiol. 74 (5), 1478–1484. http://dx.doi.org/10.1128/aem.02236-07.

Bertine, K.K., 1972. The deposition of molybdenum in anoxic waters. Mar. Chem. 1, 43–53.

Biller, D.V., Bruland, K.W., 2012. Analysis of Mn, Fe, Co, Ni, Cu, Zn, Cd, and Pb in seawater using the Nobias-chelate PA1 resin and magnetic sector inductively coupled plasma mass spectrometry (ICP-MS). Mar. Chem. 130, 12–20. http://dx.doi.org/10.1016/j.marchem.2011.12.001.

Bishop, J.K.B., Lam, P.J., Wood, T.J., 2012. Getting good particles: accurate sampling of particles by large volume in-situ filtration. Limnol. Oceanogr. Methods 10, 681–710. http://dx.doi.org/10.4319/lom.2012.10.681.

Breit, G.N., Wanty, R.B., 1991. Vanadium accumulation in carbonaceous rocks: a review of geochemical controls during deposition and diagenesis. Chem. Geol. 91, 83–97. http://dx.doi.org/10.1016/0009-2541(91)90083-4.

Brinza, L., Benning, L.G., Statham, P.J., 2008. Adsorption studies of Mo and V onto ferrihydrite. Mineral. Mag. 72 (1), 385–388. http://dx.doi.org/10.1180/minmag.2008.072.1.385.

Brinza, L., Vu, H.P., Shaw, S., Mosselmans, J.F.W., Benning, L.G., 2015. Effect of Mo and V on the hydrothermal crystallization of hematite from ferrihydrite: an *in situ* energy dispersive X-ray diffraction and X-ray absorption spectroscopy study. Cryst. Growth Des. 15 (10), 4768–4780. http://dx.doi.org/10.1021/acs.cgd.5b00173.

Brookins, D.G., 1988. Eh-pH Diagrams for Geochemistry. Spring-Verlag, New York (176 pp).

Bruland, K.W., 1983. Trace elements in sea water. In: Riley, J.P., Chester, R. (Eds.), Chemical Oceanography. Academic, London, pp. 157–220.

Bruland, K.W., Rue, E.L., Smith, G.J., DiTullio, G.R., 2005. Iron, macronutrients and diatom blooms in the Peru upwelling regime: brown and blue waters of Peru. Mar. Chem. 93 (2–4), 81–103. http://dx.doi.org/10.1016/j.marchem.2004.06.011.

Butler, A., Carter-Franklin, J.N., 2004. The role of vanadium bromoperoxidase in the biosynthesis of halogenated marine natural products. Nat. Prod. Rep. 21 (1), 180–188. http://dx.doi.org/10.1039/b302337k.

Chaigneau, A., Gizolme, A., Grados, C., 2008. Mesoscale eddies off Peru in altimeter records: identification algorithms and eddy spatio-temporal patterns. Prog. Oceanogr. 79 (2), 106–119. http://dx.doi.org/10.1016/j.pocean.2008.10.013.

Colas, F., McWilliams, J.C., Capet, X., Kurian, J., 2012. Heat balance and eddies in the Peru-Chile current system. Clim. Dyn. 39 (1), 509–529. http://dx.doi.org/10.1007/s00382-011-1170-6.

Collier, R.W., 1984. Particulate and dissolved vanadium in the North Pacific Ocean. Nature 309, 441–444.

Collier, R.W., 1985. Molybdenum in the Northeast Pacific Ocean. Limnol. Oceanogr. 30, 1351–1353.

Crans, D.C., Smee, J.J., Gaidamauskas, E., Yang, L.Q., 2004. The chemistry and biochemistry of vanadium and the biological activities exerted by vanadium compounds. Chem. Rev. 104 (2), 849–902. http://dx.doi.org/10.1021/cr020607t.

Cutter, G.A., Bruland, K.W., 2012. Rapid and noncontaminating sampling system for trace elements in global ocean surveys. Limnol. Oceanogr. Methods 10 (6), 425–436. http://dx.doi.org/10.4319/lom.2012.10.425.

Cutter, G., Andersson, P., Codispoti, L., Croot, P., Francois, R., Lohan, M., Obata, H., Rutgers v. d. Loeff, M., 2014. Sampling and Sample-Handling Protocols for GEOTRACES Cruises, v2.0. http://www.geotraces.org/libraries/documents/Intercalibration/Cookbook.pdf.

Cutter, G.A., Moffett, J.W., Nielsdóttir, M., Sanial, V., 2017. Multiple Oxidation State Trace Elements in Low Oxygen Waters off Peru: In Situ Redox Processes and Horizontal Advective/Diffusive Transport (this issue).

Dahl, T.W., Anbar, A.D., Gordon, G.W., Rosing, M.T., Frei, R., Canfield, D.E., 2010. The behavior of molybdenum and its isotopes across the chemocline and in the sediments of sulfidic Lake Cadagno, Switzerland. Geochim. Cosmochim. Acta 74 (1), 144–163. http://dx.doi.org/10.1016/j.gca.2009.09.018.

Dalai, T.K., Nishimura, K., Nozaki, Y., 2005. Geochemistry of molybdenum in the Chao Phraya River estuary, Thailand: role of suboxic diagenesis and porewater transport. Chem. Geol. 218 (3–4), 189–202. http://dx.doi.org/10.1016/j.chemgeo.2005.01.002.

Dellwig, O., Beck, M., Lemke, A., Lunau, M., Kolditz, K., Schnetger, B., Brumsack, H.-J., 2007. Non-conservative behaviour of molybdenum in coastal waters: coupling geochemical, biological, and sedimentological processes. Geochim. Cosmochim. Acta 71 (11), 2745–2761. http://dx.doi.org/10.1016/j.gca.2007.03.014.

Edmonds, H.N., German, C.R., 2004. Particle geochemistry in the Rainbow hydrothermal plume, Mid-Atlantic Ridge. Geochim. Cosmochim. Acta 68, 759–772. http://dx.doi.org/10.1016/S0016-7037(03)00498-8.

Elderfield, H., Schultz, A., 1996. Mid-ocean ridge hydrothermal fluxes and the chemical composition of the ocean. Annu. Rev. Earth Planet. Sci. 24 (1), 191–224. http://dx.doi.org/10.1146/annurev.earth.24.1.191.

Emerson, S.R., Huested, S.S., 1991. Ocean anoxia and the concentrations of molybdenum and vanadium in seawater. Mar. Chem. 34, 177–196.

Erickson, B.E., Helz, G.R., 2000. Molybdenum(VI) speciation in sulfidic waters: Stability and lability of thiomolybdates. Geochim. Cosmochim. Acta 64 (7), 1149–1158. http://dx.doi.org/10.1016/s0016-7037(99)00423-8.

Feely, R.A., Massoth, G.J., Trefry, J.H., Baker, E.T., Paulson, A.J., Lebon, G.T., 1994. Composition and sedimentation of hydrothermal plume particles from North Cleft segment, Juan de Fuca Ridge. J. Geophys. Res. Solid Earth 99, 4985–5006. http://dx.doi.org/10.1016/0012-821X(94)90023-X.

Feely, R.A., Trefry, J.H., Lebon, G.T., German, C.R., 1998. The relationship between P/Fe and V/Fe ratios in hydrothermal precipitates and dissolved phosphate in seawater. Geophys. Res. Lett. 25 (13), 2253–2256. http://dx.doi.org/10.1029/98gl01546.

Fitzsimmons, J.N., John, S.G., Marsay, C.M., Hoffman, C.L., Nicholas, S.L., Toner, B.M., German, C.R., Sherrell, R.M., 2017. Iron persistence in a distal hydrothermal plume supported by dissolved-particulate exchange. Nat. Geosci. 10 (3), 195–201. http://dx.doi.org/10.1038/ngeo2900.

Gaillardet, J., Viers, J., Dupré, B., 2014. 7.7 – Trace elements in river waters A2 – Holland, Heinrich D. In: Turekian, K.K. (Ed.), Treatise on Geochemistry, Second Edition. Elsevier, Oxford, pp. 195–235. http://dx.doi.org/10.1016/B978-0-08-095975-7.00507-6.

German, C.R., Von Damm, K.L., 2006. Hydrothermal processes. In: Holland, H., Turekian,

K.K. (Eds.), The Oceans & Marine Geochemistry. Treatise on geochemistry series, vol. 6. Elsevier, pp. 181–222.
Goldberg, T., Archer, C., Vance, D., Poulton, S.W., 2009. Mo isotope fractionation during adsorption to Fe (oxyhydr)oxides. Geochim. Cosmochim. Acta 73, 6502–6516. http://dx.doi.org/10.1016/j.gca.2009.08.004.
Goodman, B.A., Cheshire, M.V., 1975. The bonding of vanadium in complexes with humic acid: an electron paramagnetic resonance study. Geochim. Cosmochim. Acta 39, 1711–1713.
Goswami, V., Singh, S.K., Bhushan, R., 2012. Dissolved redox sensitive elements, Re, U and Mo in intense denitrification zone of the Arabian Sea. Chem. Geol. 291, 256–268. http://dx.doi.org/10.1016/j.chemgeo.2011.10.021.
Hastings, D.W., Emerson, S.R., Mix, A.C., 1996. Vanadium in foraminiferal calcite as a tracer for changes in the areal extent of reducing sediments. Paleoceanography 11 (6), 665–678. http://dx.doi.org/10.1029/96pa01985.
Hathorne, E.C., Haley, B., Stichel, T., Grasse, P., Zieringer, M., Frank, M., 2012. Online preconcentration ICP-MS analysis of rare earth elements in seawater. Geochem. Geophys. Geosyst. 13http://dx.doi.org/10.1029/2011gc003907. (n/a–n/a).
Hawco, N.J., Ohnemus, D.C., Resing, J.A., Twining, B.S., Saito, M.A., 2016. A dissolved cobalt plume in the oxygen minimum zone of the eastern tropical South Pacific. Biogeosciences 13, 5697–5717. http://dx.doi.org/10.5194/bg-13-5697-2016.
Heller, M.I., Lam, P.J., Moffett, J.W., Till, C.P., Lee, J.-M., Toner, B.M., Marcus, M.A., 2017. Accumulation of Fe oxyhydroxides in the Peruvian oxygen deficient zone implies non-oxygen dependent Fe oxidation. Geochim. Cosmochim. Acta 211, 174–193. http://dx.doi.org/10.1016/j.gca.2017.05.019.
Helz, G.R., Bura-Nakic, E., Mikac, N., Ciglenecki, I., 2011. New model for molybdenum behavior in euxinic waters. Chem. Geol. 284, 323–332. http://dx.doi.org/10.1016/j.chemgeo.2011.03.012.
Ho, T.Y., Quigg, A., Finkel, Z.V., Milligan, A.J., Wyman, K., Falkowski, P.G., Morel, F.M.M., 2003. The elemental composition of some marine phytoplankton. J. Phycol. 39, 1145–1159. http://dx.doi.org/10.1111/j.0022-3646.2003.03-090.x.
Hoffman, C.L., Nicholas, S.L., Ohnemus, D.C., Fitzsimmons, J., Sherrell, R., German, C.R., Lam, P., Toner, B.M., 2017. Near-field iron and carbon chemistry of hydrothermal plume particles, Southern East Pacific Rise 15°S. Mar. Chem (this issue: in revision).
Holland, H.D., 1984. The Chemical Evolution of the Atmosphere and Oceans. Princeton University Press, Princeton, NJ (598 pp).
Jeandel, C., Caisso, M., Minster, J.F., 1987. Vanadium behavior in the global ocean and in the Mediterranean Sea. Mar. Chem. 21, 51–74.
Jenkins, W.J., Lott III, D.E., German, C.R., Cahill, K.L., Goudreau, J., Longworth, B., 2017. The deep distributions of helium isotopes, radiocarbon, and noble gases along the U.S. GEOTRACES East Pacific Zonal Transect (GP16). Mar. Chem. http://dx.doi.org/10.1016/j.marchem.2017.03.009.
Joung, D., Shiller, A.M., 2016. Temporal and spatial variations of dissolved and colloidal trace elements in Louisiana Shelf waters. Mar. Chem. 181, 25–43. http://dx.doi.org/10.1016/j.marchem.2016.03.003.
Karstensen, J., Stramma, L., Visbeck, M., 2008. Oxygen minimum zones in the eastern tropical Atlantic and Pacific oceans. Prog. Oceanogr. 77, 331–350. http://dx.doi.org/10.1016/j.pocean.2007.05.009.
Kashiwabara, T., Takahashi, Y., Tanimizu, M., Usui, A., 2011. Molecular-scale mechanisms of distribution and isotopic fractionation of molybdenum between seawater and ferromanganese oxides. Cosmochim. Acta 75, 5762–5784. http://dx.doi.org/10.1016/j.gca.2011.07.022.
Kipp, L.E., Sanial, V., Henderson, P.B., van Beek, P., Reyss, J.-L., Hammond, D.E., Moore, W.S., Charette, M.A., 2017. Radium isotopes as tracers of hydrothermal inputs and neutrally buoyant plume dynamics in the deep ocean. Mar. Chem. http://dx.doi.org/10.1016/j.marchem.2017.06.011.
Klein, N.J., Beck, A.J., Hutchins, D.A., Sañudo-Wilhelmy, S.A., 2013. Regression modeling of the North East Atlantic Spring Bloom suggests previously unrecognized biological roles for V and Mo. Front. Microbiol. 4, 45. http://dx.doi.org/10.3389/fmicb.2013.00045.
Kowalski, N., Dellwig, O., Beck, M., Gräwe, U., Neubert, N., Nägler, T.F., Badewien, T.H., Brumsack, H.-J., van Beusekom, J.E.E., Böttcher, M.E., 2013. Pelagic molybdenum concentration anomalies and the impact of sediment resuspension on the molybdenum budget in two tidal systems of the North Sea. Geochim. Cosmochim. Acta 119, 198–211. http://dx.doi.org/10.1016/j.gca.2013.05.046.
Lam, P., Lavik, G., Jensen, M.M., van de Vossenberg, J., Schmid, M., Woebken, D., Dimitri, G., Amann, R., Jetten, M.S.M., Kuypers, M.M.M., 2009. Revising the nitrogen cycle in the Peruvian oxygen minimum zone. Proc. Natl. Acad. Sci. U. S. A. 106, 4752–4757. http://dx.doi.org/10.1073/pnas.0812444106.
Lam, P.J., Lee, J.-M., Heller, M.I., 2017. Size-fractionated distributions of suspended particle concentration and major phase composition from the U.S. GEOTRACES Eastern Pacific Zonal Transect (GP16). Mar. Chem. http://dx.doi.org/10.1016/j.marchem.2017.08.013.
Lee, J.-M., Heller, M.I., Lam, P.J., 2017. Size distribution of particulate trace elements in the U.S. GEOTRACES Eastern Pacific Zonal Transect (GP16). Mar. Chem. http://dx.doi.org/10.1016/j.marchem.2017.09.006. (this issue).
Lewan, M.D., Maynard, J.B., 1982. Factors controlling enrichment of vanadium and nickel in the bitumen of organic sedimentary rocks. Geochim. Cosmochim. Acta 46, 2547–2560.
Maia, L.B., Moura, I., Moura, J.J.G., 2017. CHAPTER 1: Molybdenum and tungsten-containing enzymes: an overview. In: Molybdenum and Tungsten Enzymes: Biochemistry. The Royal Society of Chemistry, pp. 1–80. http://dx.doi.org/10.1039/9781782623915-00001.
Manheim, F.T., 1978. Molybdenum. In: Wedepohl, K.H. (Ed.), Handbook of Geochemistry. Springer-Verlag, Berlin, pp. K1–K14.
Measures, C.I., Landing, W.M., Brown, M.T., Buck, C.S., 2008. A commercially available rosette system for trace metal-clean sampling. Limnol. Oceanogr. Methods 6, 384–394.
Michibata, H., Yamaguchi, N., Uyama, T., Ueki, T., 2003. Molecular biological approaches to the accumulation and reduction of vanadium by ascidians. Coord. Chem. Rev. 237, 41–51. http://dx.doi.org/10.1016/S0010-8545(02)00278-3.
Middelburg, J.J., Hoede, D., Van Der Sloot, H.A., Van Der Weijden, C.H., Wijkstra, J., 1988. Arsenic, antimony and vanadium in the North Atlantic Ocean. Geochim. Cosmochim. Acta 52 (12), 2871–2878. http://dx.doi.org/10.1016/0016-7037(88)90154-8.
Moffett, J.W., German, C.R., Cutter, G.A., 2015. HPLC Pigments Along the US GEOTRACES East Pacific Zonal Transect From the R/V Thomas G. Thompson TN303 Cruise in the Tropical Pacific From Peru to Tahiti During 2013 (U.S. GEOTRACES EPZT Project), Biological and Chemical Oceanography Data Management Office (BCO-DMO). Dataset Version 2015-05-15.
Moreno-Vivián, C., Cabello, P., Martínez-Luque, M., Blasco, R., Castillo, F., 1999. Prokaryotic nitrate reduction: molecular properties and functional distinction among bacterial nitrate reductases. J. Bacteriol. 181, 6573–6584.
Morris, A.W., 1975. Dissolved molybdenum and vanadium in the northeast Atlantic Ocean. Deep Sea Res. 22, 49–54.
Nakagawa, Y., Takano, S., Firdaus, M.L., Norisuye, K., Hirata, T., Vance, D., Sohrin, Y., 2012. The molybdenum isotopic composition of the modern ocean. Geochem. J. 46, 131–141. http://dx.doi.org/10.2343/geochemj.1.0158.
Nameroff, T.J., Balistrieri, L.S., Murray, J.W., 2002. Suboxic trace metal geochemistry in the eastern tropical North Pacific. Geochim. Cosmochim. Acta 66, 1139–1158. http://dx.doi.org/10.1016/S0016-7037(01)00843-2.
Nuester, J., Vogt, S., Newville, M., Kustka, A.B., Twining, B.S., 2012. The unique biogeochemicalsignature of the marine diazotroph *Trichodesmium*. Front. Microbiol. Chem. 3, 1–15.
Ohnemus, D.C., Auro, M.E., Sherrell, R.M., Lagerström, M., Morton, P.L., Twining, B.S., Rauschenberg, S., Lam, P.J., 2014. Laboratory intercomparison of marine particulate digestions including Piranha: a novel chemical method for dissolution of polyethersulfone filters. Limnol. Oceanogr. Methods 12, 530–547. http://dx.doi.org/10.4319/lom.2014.12.530.
Ohnemus, D.C., Rauschenberg, S., Cutter, G.A., Fitzsimmons, J.N., Sherrell, R.M., Twining, B.S., 2017. Elevated trace metal content of prokaryotic communities associated with marine oxygen deficient zones. Limnol. Oceanogr. 62, 3–25. http://dx.doi.org/10.1002/lno.10363.
Osterholz, H., Simon, H., Beck, M., Maerz, J., Rackebrandt, S., Brumsack, H.-J., Feudel, U., Simon, M., 2014. Impact of diatom growth on trace metal dynamics (Mn, Mo, V, U). J. Sea Res. 87, 35–45. http://dx.doi.org/10.1016/j.seares.2013.09.009.
Pegliasco, C., Chaigneau, A., Morrow, R., 2015. Main eddy vertical structures observed in the four major Eastern Boundary Upwelling Systems. Geophys. Res. Ocean 120, 6008–6033. http://dx.doi.org/10.1002/2015jc010950.
Penven, P., Echevin, V., Pasapera, J., Colas, F., Tam, J., 2005. Average circulation, seasonal cycle, and mesoscale dynamics of the Peru Current System: A modeling approach. J. Geophys. Res. 110. http://dx.doi.org/10.1029/2005jc002945.
Peters, B.D., Casciotti, K.L., Jenkins, W.J., Swift, J.H., German, C.R., Moffett, J.W., Cutter, G.A., Brzezinski, M.A., 2017. Water mass analysis of the 2013 US GEOTRACES eastern Pacific zonal transect (GP16). Mar. Chem. http://dx.doi.org/10.1016/j.marchem.2017.09.007.
Poulton, S.W., Raiswell, R., 2002. The low-temperature geochemical cycle of iron: from continental fluxes to marine sediment deposition. Am. J. Sci. 302, 774–805.
Rehder, D., 2000. Vanadium nitrogenase. J. Inorg. Biochem. 80, 133–136.
Rehder, D., 2008. Is vanadium a more versatile target in the activity of primordial life forms than hitherto anticipated? Org. Biomol. Chem. 6, 957–964. http://dx.doi.org/10.1039/b717565p.
Resing, J.A., Sedwick, P.N., German, C.R., Jenkins, W.J., Moffett, J.W., Sohst, B.M., Tagliabue, A., 2015. Basin-scale transport of hydrothermal dissolved metals across the South Pacific Ocean. Nature 523, 200–203. http://dx.doi.org/10.1038/nature14577.
Rudnick, R.L., Gao, S., 2014. 4.1 – Composition of the continental crust A2 – Holland, Heinrich D. In: Turekian, K.K. (Ed.), Treatise on Geochemistry, Second Edition. Elsevier, Oxford, pp. 1–51.
Schindelin, H., Kisker, C., Hilton, J., Rajagopalan, K.V., Rees, D.C., 1996. Crystal structure of DMSO reductase: redox-linked changes in molybdopterin coordination. Science 272 (5268), 1615–1621.
Schlitzer, R., 2015. Ocean Data View. odv.awi.de.
Scholz, F., Hensen, C., Noffke, A., Rohde, A., Liebetrau, V., Wallmann, K., 2011. Early diagenesis of redox-sensitive trace metals in the Peru upwelling area – response to ENSO-related oxygen fluctuations in the water column. Geochim. Cosmochim. Acta 75, 7257–7276. http://dx.doi.org/10.1016/j.gca.2011.08.007.
Scholz, F., Löscher, C.R., Fiskal, A., Sommer, S., Hensen, C., Lomnitz, U., Wuttig, K., Göttlicher, J., Kossel, E., Steininger, R., Canfield, D.E., 2016. Nitrate-dependent iron oxidation limits iron transport in anoxic ocean regions. Earth Planet. Sci. Lett. 454, 272–281. http://dx.doi.org/10.1016/j.epsl.2016.09.025.
Scholz, F., Siebert, C., Dale, A.W., Frank, M., 2017. Intense molybdenum accumulation in sediments underneath a nitrogenous water column and implications for the reconstruction of paleo-redox conditions based on molybdenum isotopes. Geochim. Cosmochim. Acta 213, 400–417. http://dx.doi.org/10.1016/j.gca.2017.06.048.
Scott, C., Lyons, T.W., Bekker, A., Shen, Y., Poulton, S.W., Chu, X., Anbar, A.D., 2008. Tracing the stepwise oxygenation of the Proterozoic ocean. Nature 452, 456–459. http://dx.doi.org/10.1038/nature06811.
Sherrell, R.M., Boyle, E.A., 1988. Zinc, chromium, vanadium and iron in the Mediterranean Sea. Deep Sea Res. Part A. Oceanogr. Res. Pap. 35, 1319–1334. http://dx.doi.org/10.1016/0198-0149(88)90085-4.
Shiller, A.M., Mao, L.J., 1999. Dissolved vanadium on the Louisiana Shelf: effect of oxygen depletion. Cont. Shelf Res. 19, 1007–1020. http://dx.doi.org/10.1016/s0278-

4343(99)00005-9.
Shim, M.J., Swarzenski, P.W., Shiller, A.M., 2012. Dissolved and colloidal trace elements in the Mississippi River delta outflow after Hurricanes Katrina and Rita. Cont. Shelf Res. 42, 1–9. http://dx.doi.org/10.1016/j.csr.2012.03.007.
Sohrin, Y., Urushihara, S., Nakatsuka, S., Kono, T., Higo, E., Minami, T., Norisuye, K., Umetani, S., 2008. Multielemental determination of GEOTRACES key trace metals in seawater by ICPMS after preconcentration using an ethylenediaminetriacetic acid chelating resin. Anal. Chem. 80, 6267–6273. http://dx.doi.org/10.1021/ac800500f.
Stiefel, E.I., 1996. Molybdenum bolsters the bioinorganic brigade. Science 272 (5268), 1599–1600.
Taylor, M., van Staden, J., 1994. Spectrophotometric determination of vanadium(IV) and vanadium(V) in each other's presence. Rev. Anal. 119, 1263–1276. http://dx.doi.org/10.1039/an9941901263.
Thomsen, S., Kanzow, T., Krahmann, G., Greatbatch, R.J., Dengler, M., Lavik, G., 2016. The formation of a subsurface anticyclonic eddy in the Peru-Chile Undercurrent and its impact on the near-coastal salinity, oxygen, and nutrient distributions. J. Geophys. Res. Ocean 121, 476–501. http://dx.doi.org/10.1002/2015jc010878.
Tovar-Sanchez, A., Sañudo-Wilhelmy, S.A., 2011. Influence of the Amazon River on dissolved and intra-cellular metal concentrations in *Trichodesmium* colonies along the western boundary of the sub-tropical North Atlantic Ocean. Biogeosciences 8, 217–225. http://dx.doi.org/10.5194/bg-8-217-2011.
Trefry, J.H., Metz, S., 1989. Role of hydrothermal precipitates in the geochemical cycling of vanadium. Nature 342 (6249), 531–533.
Trefry, J.H., Butterfield, D.B., Metz, S., Massoth, G.J., Trocine, R.P., Feely, R.A., 1994. Trace metlas in hydrothermal solutions from Cleft segment on the southern Jaun de Fuca Ridge. J. Geophys. Res. 99, 4925–4935. http://dx.doi.org/10.1029/93jb02108.
Tribovillard, N., Algeo, T.J., Lyons, T., Riboulleau, A., 2006. Trace metals as paleoredox and paleoproductivity proxies: an update. Chem. Geol. 232 (1–2), 12–32. http://dx.doi.org/10.1016/j.chemgeo.2006.02.012.
Tsementzi, D., Wu, J.F., Deutsch, S., Nath, S., Rodriguez-R, L.M., Burns, A.S., Ranjan, P., Sarode, N., Malmstrom, R.R., Padilla, C.C., Stone, B.K., Bristow, L.A., Larsen, M., Glass, J.B., Thamdrup, B., Woyke, T., Konstantinidis, K.T., Stewart, F.J., 2016. SAR11 bacteria linked to ocean anoxia and nitrogen loss. Nature 536 (7615), 179–183. http://dx.doi.org/10.1038/nature19068.
Tuit, C.B., 2003. The Marine Biogeochemistry of Molybdenum. Massachusetts Institute of Technology (Ph.D. Dissertation Thesis).
Tuit, C., Waterbury, J., Ravizza, G., 2004. Diel variation of molybdenum and iron in marine diazotrophic cyanobacteria. Limnol. Oceanogr. 49, 978–990. http://dx.doi.org/10.4319/lo.2004.49.4.0978.
Vorlicek, T.P., Chappaz, A., Groskreutz, L.M., Young, N., Lyons, T.W., 2015. A new analytical approach to determining Mo and Re speciation in sulfidic waters. Chem. Geol. 403, 52–57. http://dx.doi.org/10.1016/j.chemgeo.2015.03.00.
Wang, D., Sanudo-Wilhelmy, S.A., 2008. Development of an analytical protocol for the determination of V (IV) and V (V) in seawater: application to coastal environments. Mar. Chem. 112, 72–80. http://dx.doi.org/10.1016/j.marchem.2008.05.011.
Wang, D., Aller, R.C., Sanudo-Wilhelmy, S.A., 2009. A new method for the quantification of different redox-species of molybdenum (V and VI) in seawater. Mar. Chem. 117, 52–58. http://dx.doi.org/10.1016/j.marchem.2009.06.001.
Wang, D., Xia, W., Lu, S., Wang, G., Liu, Q., Moore, W.S., Arthur Chen, C.-T., 2016. The nonconservative property of dissolved molybdenum in the western Taiwan Strait: relevance of submarine groundwater discharges and biological utilization. Geochem. Geophys. Geosyst. 17, 28–43. http://dx.doi.org/10.1002/2014gc005708.
Wehrli, B., Stumm, W., 1989. Vanadyl in natural waters: adsorption and hydrolysis promote oxygenation. Geochim. Cosmochim. Acta 53, 69–77.
Wheat, C.G., Feely, R.A., Mottl, M.J., 1996. Phosphate removal by oceanic hydrothermal processes: an update of the phosphorus budget in the oceans. Geochim. Cosmochim. Acta 60, 3593–3608. http://dx.doi.org/10.1016/0016-7037(96)00189-5.
Wu, J., Wells, M.L., Rember, R., 2011. Dissolved iron anomaly in the deep tropical–subtropical Pacific: evidence for long-range transport of hydrothermal iron. Geochim. Cosmochim. Acta 75, 460–468. http://dx.doi.org/10.1016/j.gca.2010.10.024.